Beam Energy Scan II (2018–2019)

PHENIX Collaboration White Paper

OUTER HCAL

INNER HCAL

BABAR MAGNET

EMCAL

BEAMPIPE

VTX

OUTER HCAL

INNER HCAL

BABAR MAGNET

EMCAL

OUTER SILICON TRACKER

BEAMPIPE

VTX

OUTER HCAL

INNER HCAL

BABAR MAGNET

EMCAL

TPC

BEAMPIPE

VTX
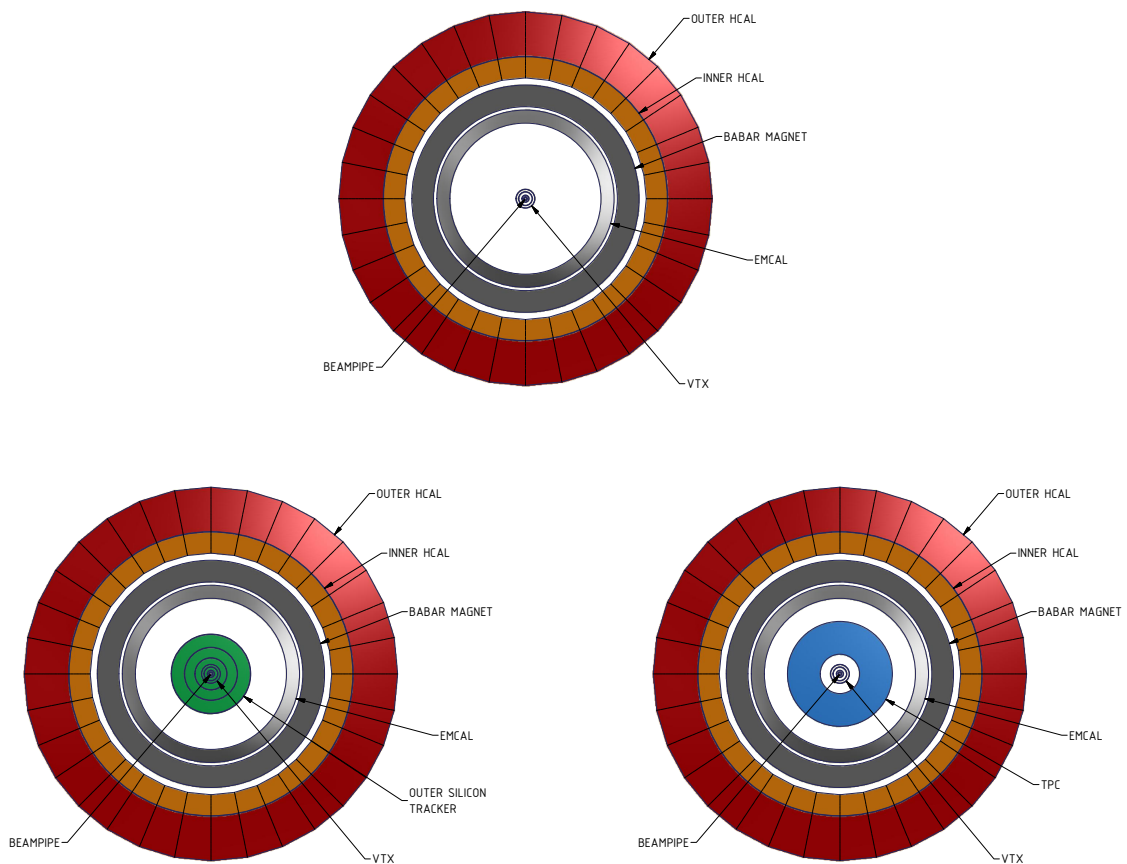
Version 1: March 1, 2014

Executive Summary

The PHENIX collaboration presents here a brief White Paper describing the plans and justification for physics running during the 2018–2019 period, referred to as the Beam Energy Scan Phase II (BES II) . This Paper is submitted in response to a charge from the Brookhaven Associate Laboratory Director — shown in Appendix A.

In 2013, a Major Item of Equipment (MIE) proposal was submitted to the DOE Office of Nuclear Physics for a extensive upgrade to the PHENIX detector. This upgrade, referred to as sPHENIX, consists of new large acceptance electromagnetic and hadronic calorimetry built around the superconducting solenoid recently acquired from the decommissioned BaBar experiment at SLAC. sPHENIX will make key new measurements of probes of the strongly coupled Quark-Gluon Plasma (sQGP) and allow for fundamental tests of our picture of its inner workings [1]. sPHENIX is expected to be complete and taking physics data in 2021.

Brookhaven Managment has developed a multi-year plan shown in Figure 1 that incorporates sequentially the completion of the so-called Midterm Upgrade Physics program from 2014–2016, the Beam Energy Scan II physics program from 2018–2019, the sPHENIX physics program with high luminosity full energy $p+p$, $p+$A, A+A from 2021–2022, and a transition to an Electron Ion Collider (EIC) in 2025. These stages are separated by periods without physics running to allow for the installation of major upgrades including a 2017 shutdown year for the inclusion of the required luminosity upgrade components for low energy running.

The BES II program is driven by the desire to understand in detail the transition from deconfined Quark-Gluon Plasma (QGP) produced at higher energies to confined hadronic resonance matter produced at lower energies. It is an experimental imperative that a careful and systematic search for a possible critical point in the QCD phase diagram be completed. To date, the PHENIX experimental acceptance has limited measurements to primarily global observables for $\sqrt{s_{NN}} < 20$ GeV [2], while the STAR experiment has a broad range of results now being published. These results give strong hints of the deconfinement transition and point to the need for definite follow up measurements in the search for the critical point. The PHENIX collaboration is excited by the prospect of contributing to this physics program with a larger acceptance in an early phase of sPHENIX. In addition, discovery of the QCD critical point would consitute a major development and its significance would be greatly enhanced by confirmation from a second experiment.

Tentative schedule for transition to eRHIC

Fiscal year	2012	2013	2014	2015	2016	2017	2018	2019	2020	2021	2022	2023	2024	2025	2026
12 GeV Upgrade															
FRIB															
RHIC/eRHIC ops		RHIC I/II operations					RHIC with LE cooling			RHIC with sPHENIX				eRHIC	
Low energy cooling															
sPHENIX - ePHENIX						sPHENIX						ePHENIX			
eSTAR												eSTAR			
eRHIC machine															
Enhanced eRHIC detector															
R&D/PED/Design (CD0-CD3)															
Projects/Construction (CD3-CD4)															
Operations/physics															

Figure 1: Brookhaven Management multi-year plan.

The executive summary from this report is as follows.

- The PHENIX detector as currently configured is projected to complete data taking at the end of the 2014–2016 period.

- From 2017–2018, there is a two-year period for decomissioning of major components of the PHENIX detector combined with the initial installation of the sPHENIX detector, including the BaBar magnetic solenoid, the hadronic calorimeter which also serves as the flux result, and a portion of the electromagnetic calorimeter.

- In 2019, the sPHENIX detector could have major components ready for commissioning as part of the BES II program, including a request for a short $p+p$ and A+A pilot run at full collision energy $\sqrt{s_{NN}} = 200$ GeV.

- An ambitious plan might include additional components for tracking and particle identification (PID) on this timeline that would enable a substantial sPHENIX BES II physics program. This plan is in the early stages and has energized the collaboration to pursue these options further.

- The options being considered do not include sufficient electron identification at low momentum to enable a dielectron program in the BES II.

For clarity, in this document we consider three detector configuration options that might be available in 2019 for data taking. These are shown in Figure 2. The first is the default configuration with the sPHENIX magnet, hadronic calorimetry, 25% of the electromagnetic calorimetry, and minimal tracking in the form of reconfiguring the existing PHENIX vertex detector pixel and strip-pixel ladders. The second option includes additional silicon

strip tracking layers funded by RIKEN that significantly improve the charged particle pattern recognition and momentum resolution. The third option forgoes additional silicon tracking layers, and instead incorporates a Time Projection Chamber (TPC) from a radius of 30–80 cm. This last option substantially extends the physics program with the inclusion of low momentum particle identification via dE/dx sampling. The design of the TPC is effectively a first stage implementation of the tracking detector considered for ePHENIX at an Electron Ion Collider [3].
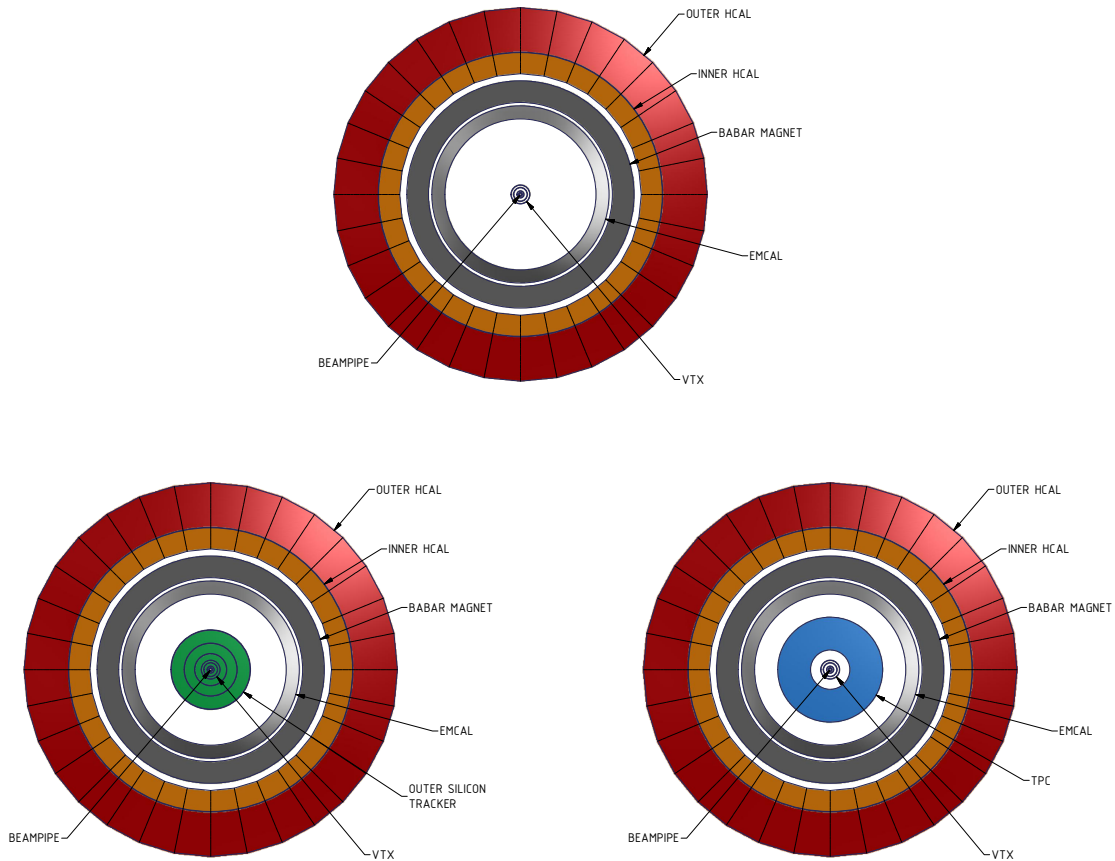
Figure 2: The diagrams show radial slices of sPHENIX with the three different detector configuration options being considered. The upper diagram depicts the MIE subsystems with the addition of the reconfigured VTX — that is, the sPHENIX baseline described in the sPHENIX proposal [1]. The lower left diagram shows sPHENIX plus an additional tracking detector consisting of three layers of silicon (layers at $r = 24, 40$, and 60 cm) located between the VTX and EMCal. The lower right diagram shows sPHENIX plus a TPC with radial extent $30 < r < 80$ cm.

These configuration options in order represent a significant increase in BES II physics capability, and at the same time increase the schedule challenges and requirement for identifying additional funding and manpower.

In this document, we present in order a review of C-AD beam luminosity projection (Chapter 1), the detector configuration details in the three options outlined above (Chapter 2), the BES II physics capabilities and projections for each option (Chapter 3), a straw-man run plan for 22-cryo weeks in 2019 that enables the BES II physics and detector commissioning for the next phase of full energy sPHENIX running (Chapter 4), and an initial timeline for decomissioning and installation over the period 2017–2019 (Chapter 5).

Contents

Chapter 1

Beam Energy Scan II Overview

As discussed in the Executive Summary, the PHENIX collaboration has been charged to detail our plans for the Beam Energy Scan Phase II (BES II) scheduled for 2018 and 2019. We have been asked to explain the scientific motivation of our proposed BES II physics program, discuss the compelling physics observables, explain the anticipated scientific reach, describe the desired run program including the requested integrated luminosities for each energy and needs for any collision species other than Au+Au, and specify any requirements for the PHENIX detector that go beyond the current equipment. We have also been asked to assess whether PHENIX could usefully contribute to a dielectron pair continuum measurement during the BES II that could in principle probe the chiral-symmetry breaking transition.

Our plan is based on the multi-year RHIC schedule (Figure 1) developed by the BNL NPP Directorate. The schedule anticipates annual RHIC running in 2014–2016 that is the typical 22–28 weeks from January to June each followed by a six month shutdown and maintenance period. The multi-year schedule anticipates a shutdown of approximately 18 months after the 2016 RHIC run, followed by the runs for the BES II in 2018 and 2019. The BES II runs are each presumed to start in January and proceed for 22 weeks, with a shutdown gap in between of 30 weeks. Following the 2019 RHIC run one foresees another 18 month shutdown followed by two years of RHIC running with the upgraded sPHENIX detector in 2021 and 2022. After the 2022 RHIC run the transition to the eRHIC facility will begin.

There are a number of additional assumptions associated with the RHIC multi-year plan that drive the conclusions and recommendations of this document. We anticipate that the upgrade of the PHENIX detector to sPHENIX will be approved and have a construction start in FY16. It will have a funding profile and technical schedule that will allow major components to be available in 2018–2019. The first part of the 18 month shutdown between the 2016 and 2018 RHIC runs will be used to decommission the existing PHENIX detector. The end of this period plus the 2018 shutdown will be used to install major components of sPHENIX. The RHIC 2019 run will be used to both commission sPHENIX and take BES II

data. The result of these assumptions and the requirements for implementing the plan are outlined in this document.

Plans are being developed to remove all detector components from the PHENIX IR during the 2016–2017 shutdown period. What would be preserved are the components necessary for the operation of the sPHENIX experiment such as the silicon vertex detector, beam pipe, carriage tracks, shield wall, electrical, water, gas and safety infrastructure. The plan foresees sufficient time during the 18 month shutdown prior to the 2018 run for the installation in 1008 of cryogenic infrastructure to support the operation of the superconducting solenoid in addition to any equipment that will be needed for the installation of sPHENIX detector components during the 2018 shutdown and operation of those components in 2019. This would include items such as custom rack platforms, rolling carriages specifically designed for sPHENIX with service umbilicals that will connect the sPHENIX detector components with the existing infrastructure. Activities in the PHENIX hall during the 2018 shutdown period will include the roll in of the sPHENIX solenoid, installation of a reconfigured VTX, partial electromagnetic calorimetry (EMCal), and a complete hadronic calorimeter (HCal) that also operates as the magnet flux return. Based on both technical issues and the anticipated sPHENIX budget profile we expect at most 25% of the EMCal to be available for the 2019 run. Any additional sPHENIX subsystems that are available at that time, such as additional outer silicon tracking layers or a Time Projection Chamber (TPC), would also get installed during this period with the goal of taking data with all installed components during the 2019 run.

The C-AD department has begun an accelerator upgrade project that will significantly enhance the luminosity of heavy ion collisions in the range $5 \leq \sqrt{s} \leq 20$ GeV. The addition of low energy electron cooling (LEReC) in the RHIC 2 o'clock area will enable the machine to increase its luminosity by a factor of 3–8 in this range of collision energies over what had previously been achieved in the first RHIC beam energy scan which took place 2010 and 2011.

Since many of the physics results from the first RHIC Beam Energy Scan were statistics limited one expects to improve the sensitivity of the physics results through an increase in luminosity plus sufficient running time. To realize the luminosity increase C-AD plans to build and install a low energy electron cooling complex over a four year period starting in 2014. First operation of the machine using LEReC is schedule for 2018. A plot showing a range of projected average luminosities for RHIC operations in BES II is shown in the left panel of Figure 1.1. The average luminosity obtained during BES I is shown by the red squares. The interaction diamond is expected to be broader at the lower collision energies. Fortunately, the pseudorapidity coverage of sPHENIX is $|\eta| \leq 1.0$, as compared to the $|\eta| \leq 0.35$ coverage of the existing PHENIX central arms, which will enable a much wider vertex cut for calorimetric measurements. Some of the physics analyses requiring charged tracks matched to the inner VTX will require a narrow vertex cut to contain events within the silicon vertex acceptance.

A cut of $|z| \leq 10$ cm will reduce the effective luminosity to 10–15% of that over the whole
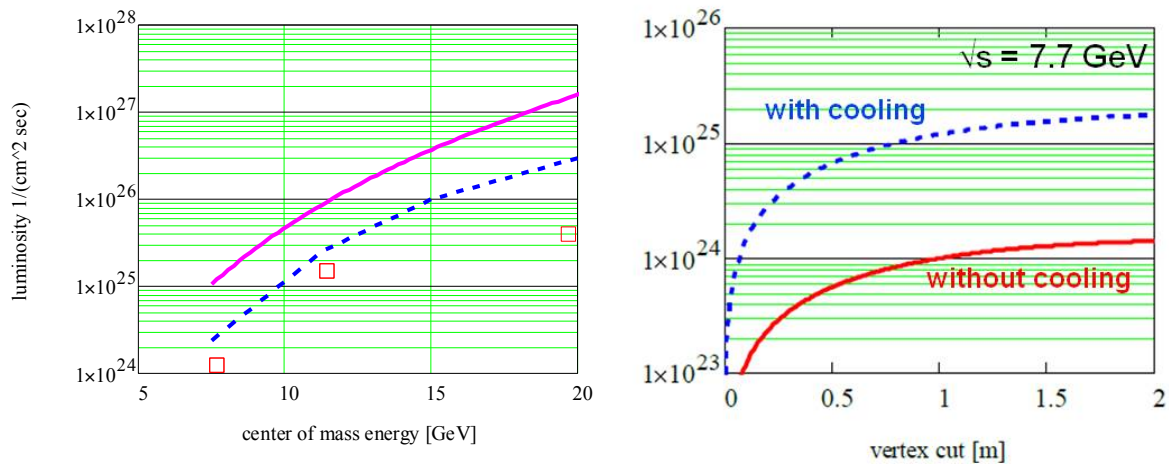
Figure 1.1: (left) RHIC luminosity vs. energy for the BES II, showing a projection of the average store luminosity within a ± 1.1 m vertex cut for 111 bunches of Au ions with electron cooling. The red squares show the measured average store luminosity achieved in BES I. The blue dashed (red solid) line indicates the minimum (maximum) improvement in luminosity expected with electron cooling. (right) Effective RHIC luminosity vs. vertex cut for $\sqrt{s} = 7.7$ GeV.

collision diamond. The effective luminosity versus vertex cut at $\sqrt{s} = 7.7$ GeV can be seen in the right panel of Figure 1.1. The reduction in effective luminosity as the vertex cut is narrowed is similar across the whole 5–20 GeV BES II energy range. These C-AD projections are utilized in constructing the physics run plan presented in this document.

Chapter 2

Detector Configuration

In this Chapter we describe the detector configuration options that might be available in 2019 during the second year of the BES II running. The decommissioning of most of the existing PHENIX detector and first stage installation of sPHENIX will be carried out in 2017–2018. Here we detail the sPHENIX calorimeter and magnet configuration expected to be available in 2019, the reconfigured silicon vertex tracker, and additional detector options including new outer silicon strip layers and a possible Time Projection Chamber (TPC).

2.1 sPHENIX Calorimetry and Magnet Configuration

Full details on the sPHENIX calorimetry and magnet are given in the sPHENIX MIE proposal [1]. Here we give a brief summary of the detector specifications and which components may be available in 2019.

The sPHENIX detector will utilize the solenoidal magnet used in the BaBar experiment [4] at SLAC, which became available after completion of the BaBar program. The paperwork for property transfer of the magnet to Brookhaven National Laboratory is now complete. The cryostat occupies the space between radii of 140 cm and 173 cm and the coil is wound at a mean radius of 153 cm for a full length of 351.2 cm. The BaBar coil operates at a nominal current of 4596 A providing 1.5 T magnetic field. The current density is varied along the length of the coil increasing at both ends by 30% via narrower windings. The main purpose of the graded current density is to maintain a high field uniformity in the bore of the solenoid.

The hadronic calorimeter (HCal) for sPHENIX also operates as the flux return for the magnet. The iron yoke of the magnetic coil is made of iron plates running parallel to the beam axis interleaved with plastic scintillator plates. The hadronic calorimeter is divided into two longitudinal compartments with the scintillators read out via embedded wavelength

shifting fiber. The hadronic calorimeter uses silicon photomultiplier sensors coupled to the fibers. The HCal has angular segmentation ($\Delta\eta \times \Delta\phi \approx 0.1 \times 0.1$). Combined with the electromagnetic calorimeter inside the cryostat, the total depth of the calorimeters is equivalent to the hadronic interaction thickness of $5\lambda_{int}$ — sufficient to fully contain the jet energy for the full range of jets produced at RHIC. The HCal is specified to have an energy resolution of order $100\%/\sqrt{E[\text{GeV}]}$.

The barrel part of electromagnetic calorimeter (EMCal) is a compact tungsten-scintillator sampling calorimeter inside the cryostat which is read out with silicon photomultipliers. The small Molière radius and short radiation length of the calorimeter allows for a high segmentation with the granularity ($\Delta\eta \times \Delta\phi \approx 0.024 \times 0.024$). At a radius of about 100 cm from the beam axis, this results in about 25,000 electronic channels read out by the same silicon photomultiplier sensors planned for use in the hadronic calorimeter. The energy resolution of the barrel part of the EMCal is approximately $12\%/\sqrt{E[\text{GeV}]}$.

Given the current project status and projected funding profile, we believe that the magnet, full hadronic calorimetry, and a partial implementation of the electromagnetic calorimetry (or order 25%) may be available for commissioing and data taking in 2019.

2.2   Reconfigured Silicon Tracking (VTX)

The current PHENIX detector includes a barrel silicon vertex tracker (VTX). The detector was commissioned in 2011 and is one of the centerpieces for data taking in 2014–2016 for measuring charm and beauty decay electrons. The VTX is comprised of two layers of pixel detectors and two layers of strip-pixel detectors. The detector covers ± 11 cm along beam line and $|\eta| < 1$ in pseudo-rapidity for collisions occurring at the center of the detector $z = 0$. The VTX covers approximately 80% of 2π in azimuth with gaps of $30°$ at twelve o'clock and six o'clock. This coverage is designed to be somewhat larger in azimuth than the existing PHENIX central arm spectrometers, where the electron identification is done.

The mechanical support structure for the VTX will need to be modified to be compatible with the sPHENIX geometry. The basic building block of the VTX is the individual ladder. The current VTX has 30 pixel ladders and 40 strip-pixel ladders. Each of these ladder works as independent detector. During the de-commissioning of PHENIX, these detector ladders will be removed from the current VTX space frame, and they will be reassembled into a new, reconfigured VTX detector that fits into sPHENIX. The reconfigured VTX will cover 2π in azimuth.

The reconfigured VTX has two pixel layers and one or two strip-pixel layers. RIKEN is now making 10 new pixel ladders. These new pixel ladders will be used to fill the existing gap in the ϕ acceptance coverage. For the strip-pixel detectors, we cannot produce more silicon modules due to limited availability of 625 μm thick high resistive silicon wafers that are needed to make the sensor. Thus the 224 sensor modules that are now in the

VTX need to be reconfigured to make new ladders and to close the gaps in ϕ coverage. The exact configuration of these ladders is not yet determined, and will also depend on the additional outer tracking discussed in the following two sections. If we keep two strip-pixel layers, we need to shrink their radii so that we can close the ϕ gaps with the same detector area coverage. Another option is to reconfigure the strip-pixel detector into a single layer. The latter option requires an additional tracking detector outside of the VTX, since three layers of silicon is not sufficient for stand-alone tracking.
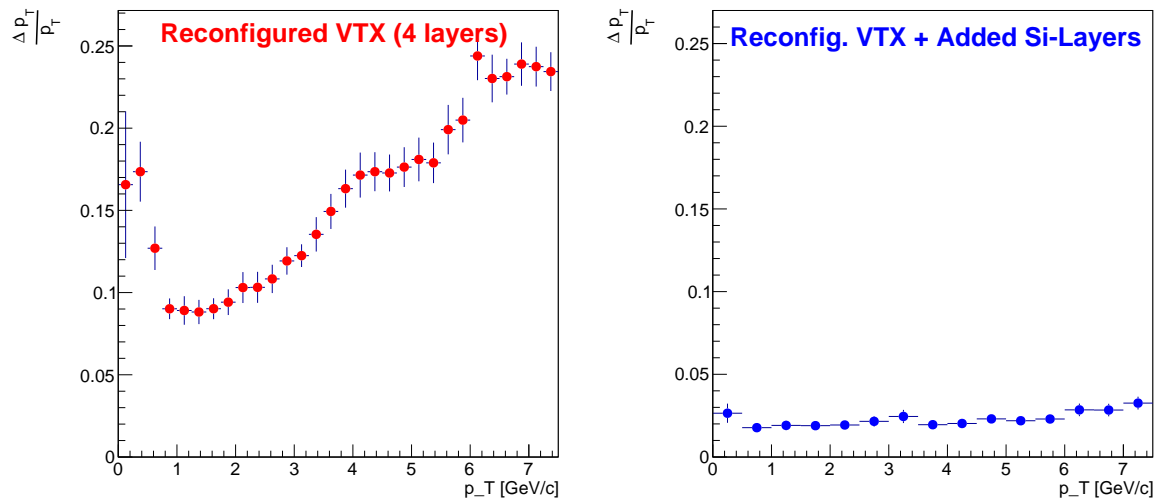

Figure 2.1: (left) GEANT-4 simulation of the momentum resolution achievable with the reconfigured VTX (assuming four layers) in the 1.5 T solenoidal field of sPHENIX. (right) GEANT4 simulation with the reconfigured VTX and additional outer strip layers.

The left panel of Figure 2.1 shows the expected performance of the reconfigured four-layer VTX detector in the new sPHENIX 1.5 T magnetic field. The resolution is approximately 10% for $p_T < 3$ GeV/c. The reconfigured VTX provides minimum tracking capability by itself. However, for the BES II physics program, the occupancies are very low so that pattern recognition is not an issue. Also, many physics analyses detailed later focus on low momentum tracks $p_T < 2$ GeV/c. For the full energy sPHENIX physics program, we require additional tracking capabilities which have been part of the plan from the outset.

2.3   Additional Outer Silicon Tracking Option

The above described sPHENIX detector configuration has only the reconfigured VTX for charged particle tracking. The detector provides minimum tracking capability and limited momentum resolution ($\sigma_p/p \approx 10\%$). An additional tracking detector located outside of the reconfigured VTX will substantially improve the tracking capability of sPHENIX, which is crucial for full energy running.

One of two options considered as the additional tracking detector is an outer silicon tracker. The concept is to add more layers of silicon strip detectors outside of the reconfigured VTX. The RIKEN group has been pursuing this option and is actively seeking funds from Japanese agencies for the construction of the detector.
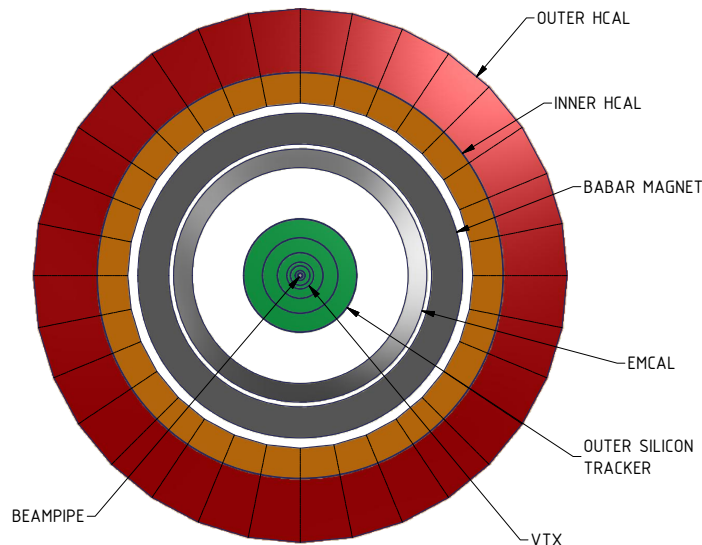

Figure 2.2: Cross section of the sPHENIX detector with an outer silicon tracker (shown in green).

Figure 2.2 shows an engineering rendering of the outer silicon detector in position within the sPHENIX configuration. It comprises three new layers of single-sided silicon strip detectors. The detector covers $|\eta| < 1$ and 2π in azimuth. The basic building block of the detector is a silicon module made of a single-sided strip sensor and a Read Out Card (ROC). The sensor is approximately 10 cm $\times$ 10 cm, and has 1280 strips with 75μm strip pitch. It is read out by ten SVX4 read-out chips. The SVX4 has been used by PHENIX in the strip-pixel detector of the VTX, and is incorporated into the design of the MPC-EX upgrade detector project as well. Thus PHENIX has substantial experience with the chip. A ladder is made of several sensor modules, a stave that provides mechanical support and cooling to the modules, and a read-out bus connecting them. Several ladders would be assembled into a barrel to cover 2π in azimuth. Three such layers makes the outer silicon tracker. In order to cover $|\eta| < 1$, the length of the ladders would increase as one goes out in radius .

One configuration of the outer silicon tracker is summarized in Table 2.1. The total number of silicon modules in the tracker is 1038, corresponding to the total area of silicon of approximately 10 m^2. In comparison, the strip-pixel detector in the current PHENIX VTX

Table 2.1: Dimensions for the configuration of the outer silicon tracker. For each of three layers, its radius R, half length Z of the ladder, the number of silicon modules (SMs) per ladder, the number of ladders per layer, the total number of SMs in the ladder, and the radiation length of the layer are shown.

Layer	R(cm)	Z (cm)	SM/ladder	Ladder	total SM	rad. length
B3	24	±35	7	16	112	1%
B4	40	±55	11	26	286	1%
B5	60	±80	16	40	640	1%
Total				82	1038	3%

has 40 ladders and 224 silicon modules. The outer tracker is larger than the existing strip-pixel system. However, since it is made of conventional single-sided strips, it is less complicated than the strip-pixel detector, which uses a novel strip-pixel sensor with 2-dimensional read-out.

The momentum resolution of a total of six layers, including the reconfigured VTX and additional outer strip layers, has been evaluated within the GEANT4 framework for sPHENIX. The results are shown in the right panel of Figure 2.1. The improvement in the momentum resolution is readily apparent. In addition, for full energy running, the additional layers are crucial for pattern recognition in high occupancy events and for displaced vertex analyses. It is envisioned that the strip layers will provide some dE/dx information, though this has not yet been evaluated for particle identification purposes.

The RIKEN group plans to start R&D and prototyping of the silicon module for the outer silicon detector in the next Japanese fiscal year (JFY2014), which begins April 2014. The goal is to make a prototype of the large, 10 cm × 10 cm silicon sensors, develop prototype ROCs, and construct a prototype module composed of sensors plus stave and ROC.

2.4   Time Projection Chamber (TPC) Option

The other solution being considered for the additional tracking needed in the sPHENIX central barrel is a fast, compact Time Projection Chamber (TPC). The TPC would sit in the radial space between the reconfigured vertex detector and EMCal as shown in Figure 2.3.

The longitudinal dimension of the central tracking system is 100 cm in each direction,
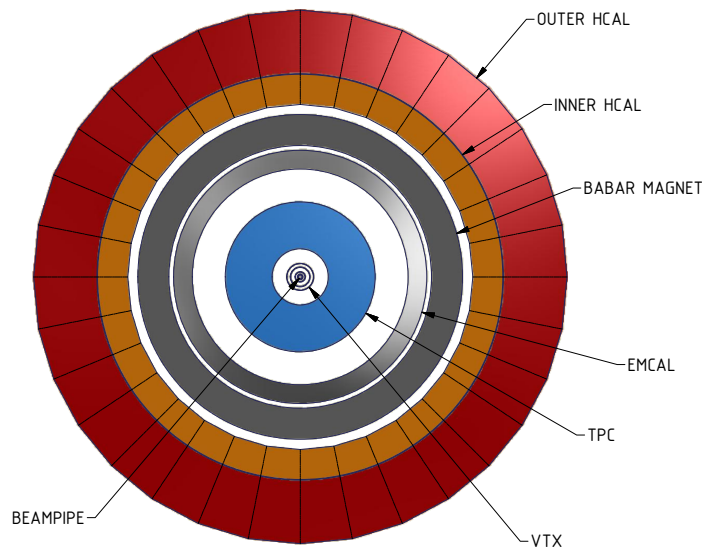
Figure 2.3: Cross section of the sPHENIX detector with the reconfigured VTX and a Time Projection Chamber (shown in blue).

providing the maximum number of measured space points for the tracks with $|\eta| < 1$. The TPC is immersed in the uniform 1.5 T solenoidal magnetic field of the BaBar magnet. The momentum resolution of the combined reconfigured VTX and the TPC is shown in Figure 2.4.

The TPC determines the transverse momentum of the track with an accuracy of 0.5% at $p_T \approx 1 \, \text{GeV}/c$. Below that momentum the resolution is affected by the material preceding the TPC, which is assumed equal to 13% of radiation length. Above that p_T the resolution decreases with momentum, but stays below 2% for almost all detector configurations even at p_T =10 GeV/c. Increasing the outer radius from 80 cm to 95 cm improves the momentum resolution by approximately 15%. The outer radius of a compact TPC will be determined in part by plans for future upgrades of sPHENIX and ePHENIX.

Spatial resolution in the transverse plane plays crucial role in determining the track p_T. Several conditions are required to achieve the high resolution in the measurement of the transverse coordinates of the space points left by a track. High granularity of the detector is needed as well as small diffusion of the primary ionization in the gas. Further, the intrinsic resolution of the read-out system must be sufficient to preserve the position of the electron cloud arriving at the detector read-out plane.

Read-out elements adequate to the goal are micro pattern detectors such as gas electron multiplier (GEM), Micromega or a combination of the two. GEMs are thin foils that transfer
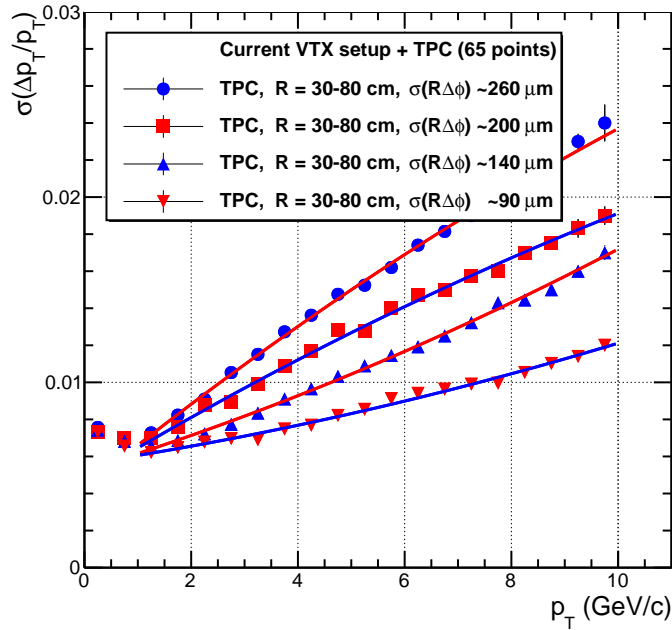
Figure 2.4: p_T resolution of the TPC with 65 circular pad rows as a function of p_T The calculation is for a TPC with inner radius of 30 cm and an outer radius of 80 cm.

multiplied ionization from one side to another and therefore can be used in stages. This significantly increases the detector stability in the environment of heavy ion collisions where slow particles can deposit initial ionization exceeding by orders of magnitude ionization from minimum ionizing particles.

Working gases considered for the TPC are the CF_4-based gas mixtures. At an electric drift field of $\sim 1\,kV/cm$, initial ionization in the gas propagates at drift velocity up to $10\,cm/\mu s$. These gas mixtures have the smallest diffusion of gases used in TPCs. The strong magnetic field of the coil further freezes transverse diffusion of the primary ionization. The CF_4-based gases require higher working voltages for the same gas gain compared to most other gas mixtures. This does not pose a problem for the multi-GEM read-out configuration.

The CF_4-based gas mixtures compared have large primary ionization, providing the ability to accurately measure dE/dx along the track and identify the particle which produced it. In pure CF_4, a minimum ionizing particle produces ~ 100 electron-ion pairs per centimeter. Measuring the charge of the primary ionization enables the separation of electrons from pions above approximately $200\,MeV/c$, pions from kaons below $1\,GeV/c$ and kaons from protons up to $1.5\,GeV/c$. Figure 2.5 shows PID separation lines in numbers of combined standard deviations as a function of particle p_T. The band assumes that the accuracy of the dE/dx determination for a full track is from 5–10%. Although a more accurate assessment of PID performance requires a more realistic Monte-Carlo than currently available, it can be compared with the measured 8% resolution reported by the STAR collaboration [5].

One of the main obstacles faced in the construction of the TPCs for heavy ion experiments
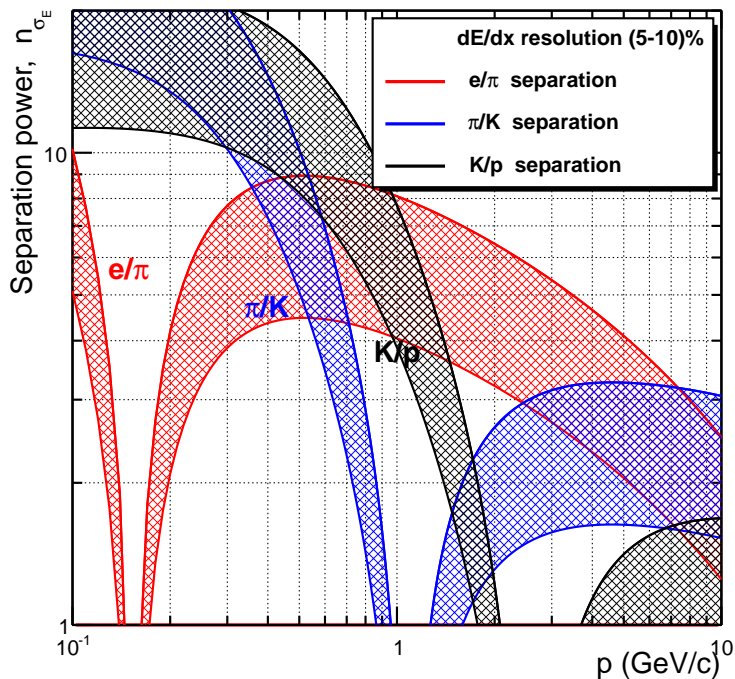
Figure 2.5: Particle identification capabilities of the dE/dx technique. The bands correspond to 5–10% resolution in the measurement of the charge for a fully reconstructed track.

is the performance limitation coming from the build up of space charge. Positively charged ions, produced in the gas amplification process, drift back into the volume of the TPC and build up a cloud of free charge which alters the speed and trajectories of drifting electrons. Recent studies made by several research groups [6] show that this can be overcome by choosing proper voltages on the layers of GEMs.

This option is attractive in that one adds particle identification capability to sPHENIX during the BES II phase and beyond. The detector would also have a larger acceptance in the longitudinal coordinate of the collision. At low energy Au+Au running, the collision diamond is very large and the current PHENIX VTX only has full acceptance for vertices within ±10 cm of the detector center. Another consideration is that the TPC is one of the tracking solutions being actively pursued for the ePHENIX detector that is under study as an Electron Ion Collider (EIC) detector. Significant additional funding would need to be identified for this scenario and there are timeline challenges for physics running by 2019. Regardless of the scenario chosen for sPHENIX tracking, one expects a very active program to develop such a detector for EIC.

Chapter 3

Physics Goals for the BES II

The ability of the RHIC machine to provide Au+Au collisions covering more than an order of magnitude variation in $\sqrt{s_{NN}}$ enables an exciting program of studying the QCD phase diagram over a broad range of net baryon density (μ_B). The program of the BES II is fundamentally focussed on making definitive physics conclusions regarding the onset of deconfinement and the possibility of a critical end point in the phase diagram, following up on exciting initial results from the successful lower luminosity BES I program.

The location of the phase boundaries and the critical end point (CEP), in the plane of temperature versus baryon chemical potential (T, μ_B), are fundamental characteristics of the phase diagram [7]. Lattice QCD calculations suggest that the quark-hadron transition is a crossover at high temperature (T) and small μ_B or high collision energy $\sqrt{s_{NN}}$ [8]. For larger values of μ_B or lower $\sqrt{s_{NN}}$, several model calculations have indicated a first order transition [9, 10] and hence, the possible existence of a CEP. In the BES II, PHENIX aims to validate the essential "landmarks" of the phase diagram, as well as to extract the properties of each QCD phase.

In this Chapter, we detail the possible physics measurement capabilities depending on the PHENIX detector configuration available. With the reconfigured silicon vertex tracker and potential additional layers, one can measure unidentified hadrons over a large acceptance. This enables for example measurements of charge separation with respect to reaction plane which is sensitive to the chiral magnetic effect, that requires a deconfined medium. If the Time Projection Chamber tracking option is realized, particle identification based on dE/dx would be possible. This enables for example measurements of the net proton fluctuations that are proposed as a sensitive probe of the critical point.

Table 3.1 gives a summary of physics topics that may be available to sPHENIX in the BES II program. The number of event estimates are to make a significant measurement in the 10% most central bin in Au+Au at $\sqrt{s_{NN}} = 19$ GeV. For example, the particle spectra requires enough events to record more than 10 counts per 0.2 GeV/c wide p_T bin up to 3 GeV/c. The last column details the requirements in terms of detectors, for example the reconfigured silicon tracking (VTX) and/or the Time Projection Chamber (TPC).

Table 3.1: A summary of physics topics potentially accessible with the PHENIX detector (depending on the configuration) for the BES II program including an estimate of the minimum number of events necessary to make a statistically significant measurement in the 10% most central bin for Au+Au at $\sqrt{s_{NN}} = 19$ GeV.

Physics Analysis	N_{evt} ($\times 10^6$)	Required Detectors
Charged Particle Multiplicity	5	VTX and/or TPC
Multiplicity Fluctuations	5	VTX and/or TPC
Charged Particle p_T Spectra	10	VTX and/or TPC
p_T Fluctuations	10	VTX and/or TPC
Moments of Net Charge	10	VTX and/or TPC
Charged Particle Flow	10	VTX and/or TPC
Charged Particle R_{CP}	30	VTX and/or TPC
Di-hadron Correlations	50	VTX and/or TPC
Chiral Magnetic Effect	10	VTX and/or TPC
Transverse Energy	5	EMCal
Neutral Pion Spectra	10	EMCal
Neutral Pion R_{CP}	30	EMCal
Identified Particle Spectra	10	TPC
Identified Particle Ratios	10	TPC
Identified Particle Flow	30	TPC
Identified Particle HBT	50	TPC
Moments of Net Protons	100	TPC
Particle Ratio Fluctuations ($K/\pi,\overline{p}/p$)	100	TPC

3.1   Global Variables

Although the measurements of charged particle multiplicity and transverse energy production are not considered to be sensitive observables for the detection of the QCD critical point, these observables are closely related to the geometry of the system and are important for characterizing the global properties of the colliding system. The Bjorken energy density [11] can be estimated from the transverse energy as follows:

$$\epsilon_{BJ} = \frac{1}{A_\perp \tau} \frac{dE_{\mathrm{T}}}{dy}, \tag{3.1}$$

where τ is the formation time and $A_\perp$ is the transverse overlap area of the nuclei. PHENIX has preliminary measurements of both $dN/d\eta$ and $dE_T/d\eta$ at 7.7, 19.6, 27, and 39 GeV [12].
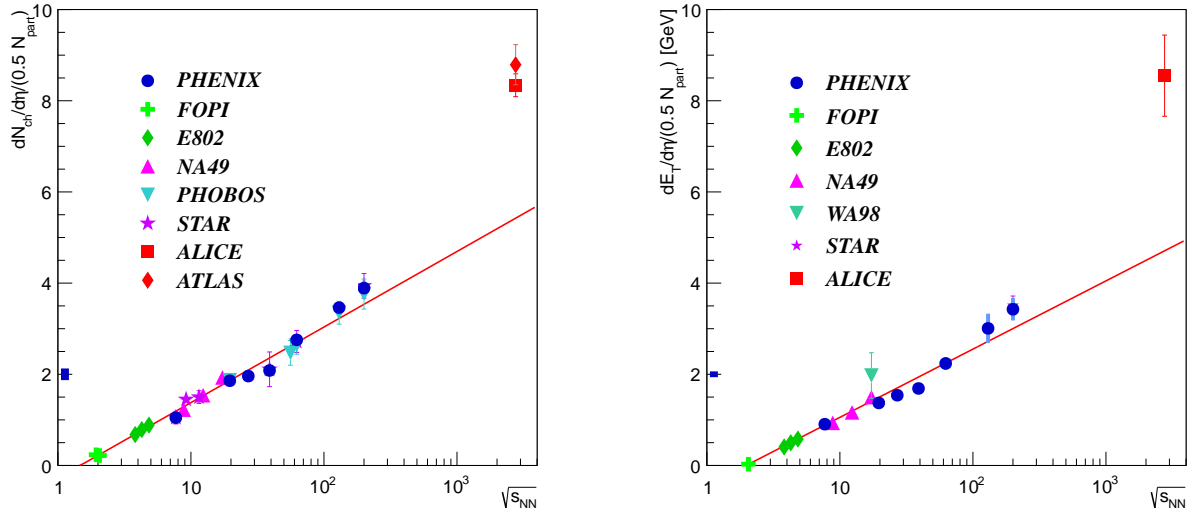
Figure 3.1: (left) The value of $dE_T/d\eta$ at mid-rapidity normalized by the number of participant pairs as a function of $\sqrt{s_{NN}}$ for 0–5% central Au+Au collisions. The red line is an exponential fit to all of the data points excluding the ALICE point [13]. (right) The value of $dN_{ch}/d\eta$ at mid-rapidity normalized by the number of participant pairs as a function of $\sqrt{s_{NN}}$ for 0–5% central Au+Au collisions. The red line is an exponential fit to all of the data points excluding the ALICE and ATLAS points [13]. In both panels, the point near the left edge of the plot indicates the scale of the systematic uncertainty on the PHENIX data points.

Both observables increase monotonically over this range as $\sqrt{s_{NN}}$ increases as seen in Figure 3.1.

The measurement of transverse energy is possible using a partial implementation of the electromagnetic calorimeter (EMCal) and the full hadronic calorimeter (HCal). The measurement of charged particle multiplicity is possible using the reconfigured VTX detector alone. It is estimated that at least 5 million events are needed to make these measurements at each energy. It is important to make this measurement at any collision energy for which PHENIX has not taken data. At energies where PHENIX has previously taken data in BES I, these measurements would serve as an excellent cross-check, especially for commissioning the EMCal and HCal energy scales.

3.2   Spectra and Nuclear Modification Factors

A wealth of necessary information about the system can be obtained from measurements of the transverse momentum spectra of various identified particle species. A blast wave function can be fit to the spectra to obtain the kinetic freeze-out temperature and mean transverse velocity of the hadrons in the medium [14]. Measurements of the freeze-out

temperature exhibit a saturation, or plateau, starting at $\sqrt{s_{NN}} \approx 8\text{--}12$ GeV that extends to 200 GeV. It has been speculated that this indicates the system is creating a mixed phase at these energies [15].

The transverse momentum spectra and their ratios for various particle species can be used to estimate the location of the system on the QCD phase diagram. A statistical thermal model can be used to estimate the values of the chemical freeze-out temperature and the baryon chemical potential [16]. The STAR experiment has observed a centrality dependence of the freeze-out temperature as a function of the baryon chemical potential for collision energies below 39 GeV. Isolation of the energy where this effect begins to manifest itself could help provide information about the location of the critical point.

One of the most prominent signatures of the QGP is that of jet suppression at the upper RHIC energies. There is an absence of reference $p+p$ data at all of the energies covered by the RHIC beam energy scan programs, but the magnitude of the suppression can still be estimated by replacing the R_{AA} measure with R_{CP}, defined as follows:

$$R_{CP} = \frac{N_{binary,peripheral}}{N_{binary,central}} \times \frac{\frac{d^2N}{p_T dp_T d\eta}\big|_{central}}{\frac{d^2N}{p_T dp_T d\eta}\big|_{peripheral}}. \tag{3.2}$$

PHENIX has measured the suppression of neutral pions [17] and J/ψ particles [18], showing that the suppression persists down to $\sqrt{s_{NN}} = 39$ GeV. Preliminary STAR measurements indicate that the suppression of charged hadrons begins to manifest above $\sqrt{s_{NN}} = 27$ GeV, as shown in Figure 3.2 [19]. It is important to continue the study of the evolution of R_{CP} for more collision energies and to confirm the STAR results with a PHENIX measurement.

For BES II, PHENIX will be able to measure the p_T spectra and R_{CP} of unidentified charged hadrons using the reconfigured VTX detector. The addition of the EMCal will enable PHENIX to measure the spectra and R_{CP} of neutral pions. The measurement of identified particle spectra enabling an estimate of the freeze-out temperature and baryon chemical potential will only be available with the addition of a TPC. The TPC will have dE/dx particle identification capabilities up to approximately 1 GeV/c, which is sufficient coverage at these energies.

In principle it would be desirable to have $p+p$ measurements at the same collision energies to compute R_{AA}, as opposed on only R_{CP}. However, the RHIC projections for the averaged delivered luminosity per week for $p+p$ are 0.02 pb^{-1} at 7.7 GeV, 0.24 pb^{-1} at 13.5 GeV, and 0.86 pb^{-1} at 19.6 GeV. In order to record a sufficient data set for R_{AA} measurements would require 275, 23, and 6 weeks at the respective energies. Given the constraints in available running time, we do not include any such request in this document.
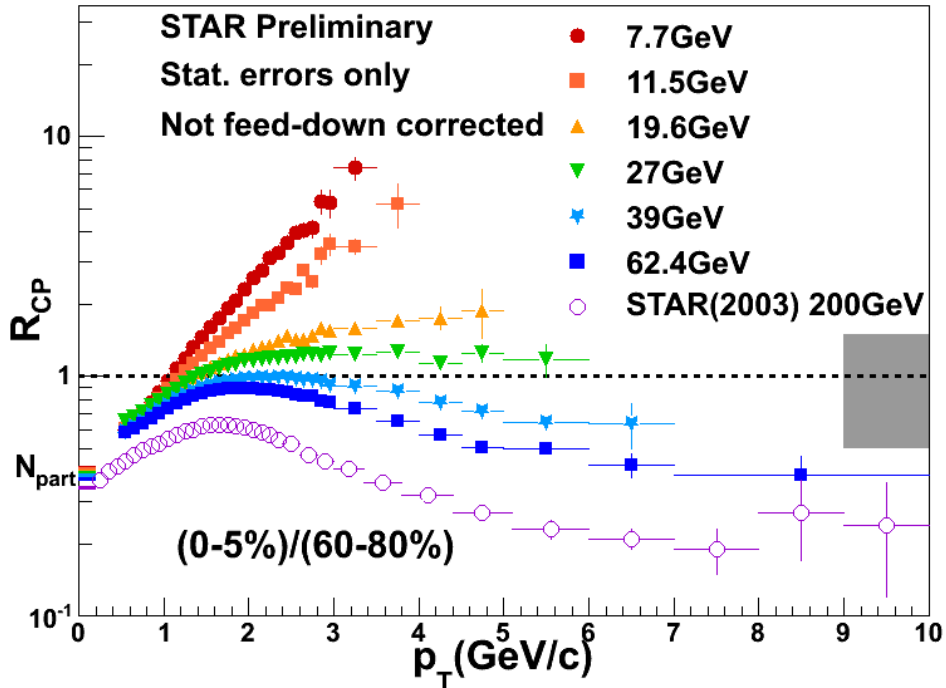
Figure 3.2: Preliminary charged hadron R_{CP} as a function of centrality for Au+Au collisions at a variety of collision energies as measured by the STAR Collaboration [19].

3.3   HBT and Flow

One of our strategies for experimental study of the phase diagram is centered on the measurement of flow and HBT excitation functions. These excitation functions will be used to extract the properties of the QCD phases and to carry out a comprehensive search for the CEP and the phase boundaries over a broad range of μ_B and T values.

Our proposed analysis of these excitation functions is three-pronged. First, we will use flow excitation functions for both odd and even v_n, to map the (μ_B, T) dependence of flow fluctuations and search for a possible characteristic enhancement. That is, we will identify and extract v_n fluctuations over and above those driven by initial-state geometry fluctuations [20], and use them to search for the onset of critical fluctuations which are thought to be one of the more important stationary state signals for locating the CEP.

In the vicinity of the critical point, the expansion dynamics of the fireball could be altered and this might leave an imprint on the magnitude of the space-time extent of the emitting system. That is, decay trajectories close to the CEP could give much larger space-time extents because of a "softening" of the equation of state (i.e. the sound speed $c_s \sim 0$). Therefore, a second avenue is to use the HBT excitation functions to make a detailed map of the space-time extent of the emitting systems as a function of μ_B and T.

For the third aspect, we aim to map the μ_B and T dependence of the ratio of viscosity to

entropy density, η/s. In prior work [21], it has been argued, by analogy to atomic and molecular substances, that the CEP could be signaled by a minimum in the dependence of $4\pi\eta/s$ on the reduced temperature $t = (T - T_c)/T_c$ and a relatively sharp increase in $\langle 4\pi\eta/s \rangle$ vs. μ_B for $t > 0$. In a recent phenomenological study [22], the viscous coefficients β'', which encode the magnitude of η/s, were extracted as a function of $\sqrt{s_{NN}}$ and found to show a tantalizing pattern of viscous damping [albeit with sizable error bars] suggestive of the expected variations of η/s in the temperature-baryon chemical potential (T, μ_B) plane. Further detailed measurements with BES II would not only provide a unique set of measurements for mapping the μ_B and T dependence of η/s, but also facilitate a search for the expected signatures for the CEP.

3.4   Chiral Magnetic Effect

The hypothesized Chiral Magnetic Effect (CME) is not a characteristic of the QGP, per se, but rather an expression of an underlying local imbalance of chirality which is a fundamental characteristic of QCD. The QCD vacuum exists as a superposition of states of differing Chern-Simons winding number. Spontaneous topological transitions between states (tunneling events via instantons and hopping events via sphalerons) are frequent. High diffusion rates are calculated at strong-coupling via AdS/CFT duality [23] and also observed in real-time lattice simulations [24, 25].

Heavy ion collisions provide a unique environment for the observation of topological charge fluctuations by providing both a deconfined state (sQGP) and a strong magnetic field in non-central collisions ($\sim 10^{17}$ Gauss). The magnetic field, with known orientation perpendicular to the reaction plane, along with the local imbalance of chirality results in charge-dependent free quark migration that induces a net electric dipole moment of the sQGP along the magnetic field direction. This dipole moment can be indirectly observed by a comparison of like-sign and unlike-sign charged particle correlations.

Currently, observations of the Chiral Magnetic Effect are limited by the fact that the only known measure of the parity-odd physics is a parity-even observable. This fact allows any conservation law (e.g. momentum conservation) to generate false positive signatures. Nonetheless, continued development of CME measurements and their dependence upon a variety of experimental parameters (such as centrality or $\sqrt{s}$) yield intriguing physics and perhaps a secondary measure of the onset of deconfinement.

Measurements with unidentified charged hadrons of the charge separation with respect to the reaction plane are achievable with the larger sPHENIX acceptance utilizing either the reconfigured silicon tracking or with the enhanced tracking options.

Table 3.2: Experimental definitions for higher moments the lattice susceptibilities to which they correspond.

moments	experimental definitions	lattice susceptibilities
σ_q^2 / M_q	$\frac{\langle (\delta N_q)^2 \rangle}{\langle N_q \rangle}$	$\chi_q^{(2)} / \chi_q^{(1)}$
$S_q \sigma_q$	$\frac{\langle (\delta N_q)^3 \rangle}{\sigma^2}$	$\chi_q^{(3)} / \chi_q^{(2)}$
$\kappa_q \sigma_q^2$	$\frac{\langle (\delta N_q)^4 \rangle}{\sigma^2} - 3\sigma^2$	$\chi_q^{(4)} / \chi_q^{(2)}$

3.5   Fluctuations and Analysis of Higher Moments

Event-by-event fluctuations of thermodynamic quantities offer the most direct evidence for the presence of a critical endpoint in the T-μ phase diagram [26] and are expected to exhibit non-monotonic behavior as a control parameter such as the beam energy is varied across the region of the critical point. Fluctuations of charge, strangeness, and baryon number are sensitive to the coherence length, ξ, which diverges as the critical point is approached. Fluctuation measurements have the additional advantage that they can be directly related to the susceptibilities, $\chi_q^{(n)} = \frac{\partial^n (p/T^4)}{\partial (\mu_q/T)^n}$, that can be calculated in Lattice QCD [27]. By taking ratios, volume effects are canceled, however, the divergence of the coherence length is limited by the relatively brief period that the heavy ion collision spends in the vicinity of the critical point before freeze-out. Estimates for the maximum value that can be attained in a heavy ion collision are in the range $\xi =$ 2–3 fm [28]. For this reason, we are most interested in measuring the higher moments, the third order skewness and fourth order kurtosis are proportional to $\xi^{\frac{9}{2}}$ and ξ^7, respectively, and therefore may show significant deviations for heavy-ion evolutions that pass sufficiently close to the critical point [29]. The experimental definitions for the first three ratios of moments and their corresponding susceptibility ratios are listed in Table 3.2.

Despite the attractiveness of fluctuation measurements as a probe of equilibrium dynamics, one must consider remnant contributions from the initial state fluctuations, particle conservation effects, and the influence of late state re-scattering effects. Recent calculations indicate that these effects are likely to be small [30]. Furthermore, among the quantities listed in Table 3.2, only the net charge fluctuations can be measured experimentally. However, because the sigma field does not couple to isospin, the proton number fluctuation is directly connected to baryon number fluctuation as well as the charge fluctuation [31]. Therefore measurements of the net proton moments have attracted the greatest interest, although evidence for the critical point should also be present in the charge fluctuations.
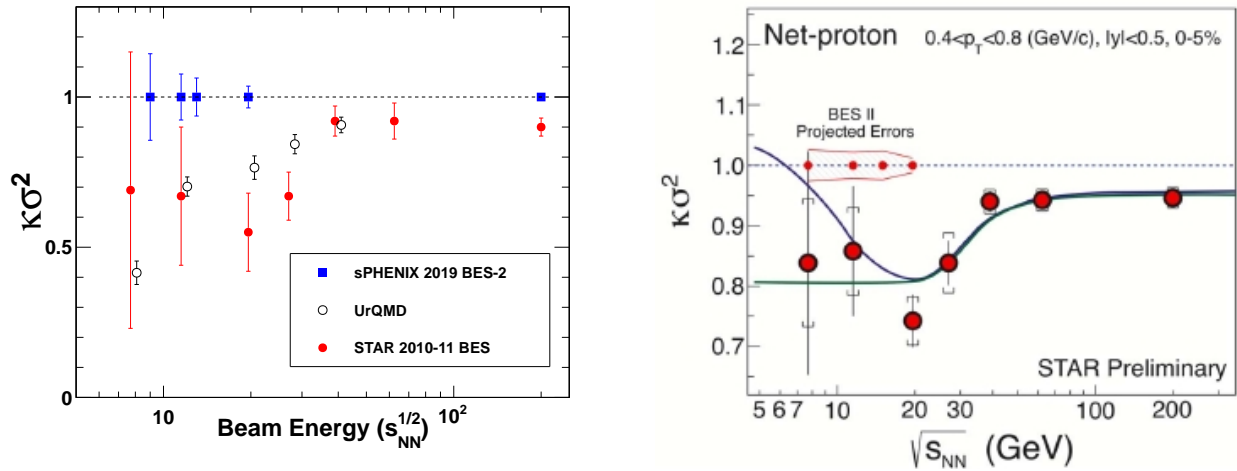
Figure 3.3: Estimates for sPHENIX sensitivity to measurement of net proton $\kappa\sigma^2$ for Au+Au collisions as a function of $\sqrt{s_{NN}}$ are shown on the left panel, and similar estimates for STAR are shown on the right panel. Both estimates are compared the published STAR results from the first beam energy scan. See text for details.

3.5.1   Net Proton Fluctuations

With the benefit of a TPC, described in Section 2.4, sPHENIX will have the capability to perform meaningful measurements and significantly improve upon the published results for BES I. Figure 3.3 shows the value of $\kappa\sigma^2$ for net proton fluctuations measured by STAR during the first beam energy scan (BES I) [32], along with projected uncertainties for BES II, for which RHIC instantaneous luminosities are expected to increase by a factor of 3 to 8 over a range in collision energies from $\sqrt{s} = 5$–20 GeV. Though the results from STAR are intriguing, they are limited by statistics and have been shown to be consistent with UrQMD calculations. Repeating these measurements with significantly higher statistics is one of the main objectives of BES II. The sPHENIX measurement in 2019 will have similar uncertainties (see Figure 3.3) to those projected by the STAR experiment for physics signals not requiring a narrow vertex cut.

3.5.2   Net Charge Fluctuations

Near the QCD critical point, it is expected that fluctuations of charged particle multiplicity and net charge per event will increase [26]. PHENIX has measured charged particle multiplicity fluctuations, expressed in terms of the scaled variance $\omega_{ch} = \sigma_{ch}^2/\mu_{ch}$ at 200 GeV, 62.4 GeV, 39 GeV and 7.7 GeV. This quantity does not change significantly at any of the energies PHENIX has measured, as shown in Figure 3.4.

A more sensitive probe for the presence of the QCD critical point is the measurement of the
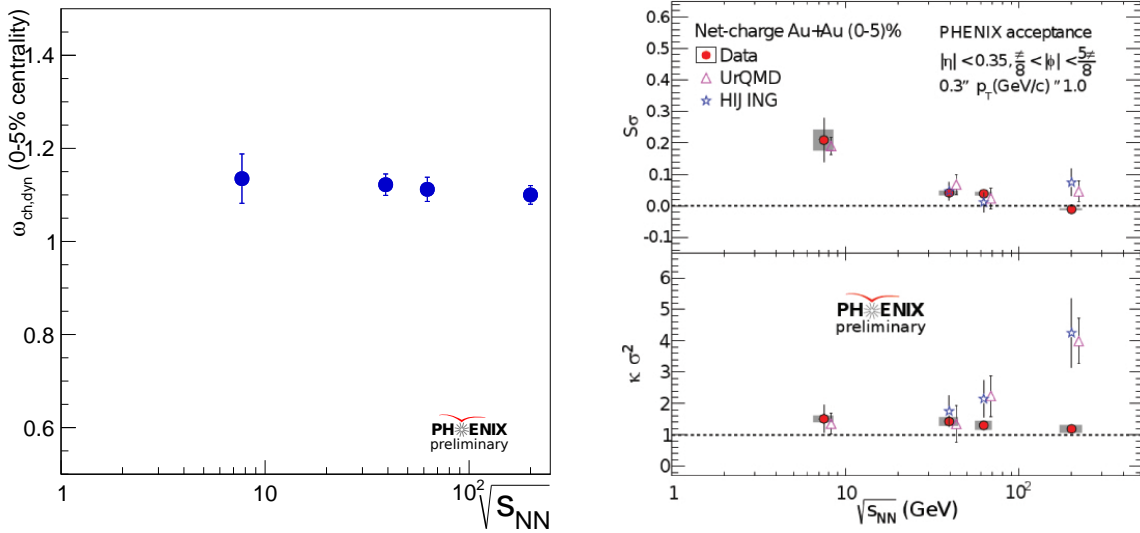
Figure 3.4: (left) Multiplicity fluctuations in 0–5% central collisions expressed in terms of the scaled variance measured by PHENIX. The fluctuations have been corrected for non-dynamic geometry fluctuations. (right) The skewness multiplied by the standard deviation and the kurtosis multiplied by the variance from net charge distributions from central Au+Au collisions. The circles represent the data. The gray error bars represent the systematic uncertainties. Also shown are UrQMD and HIJING simulation results processed through the PHENIX acceptance.

moments of the net charge distribution. PHENIX has measured the skewness and kurtosis for central collisions, as shown in Figure 3.4 as a function of $\sqrt{s_{NN}}$. The data are compared to UrQMD and HIJING simulation results processed through the PHENIX acceptance and detector response. There is no excess above the simulation results observed in the data at these four collision energies. Extending these measurements to additional energies and with larger statistics is achievable in the BES II.

3.6   Low-mass Dileptons

The BES II white paper charge (see Appendix A) contains a specific request to assess the detector capabilities for low-mass dilepton measurements at collision energies where the chiral symmetry breaking transition may be probed. Although it would be desirable to investigate the onset of deconfinement by measuring the di-electron spectra using the EMCal, the measurement is not possible without the addition of a detector designed for electron identification with high purity. The combination of the EMCal and TPC does not provide sufficient e/π separation to make a measurement of the di-electron spectrum with sufficient sensitivity. Since a RICH detector of comparable performance to PHENIX cannot
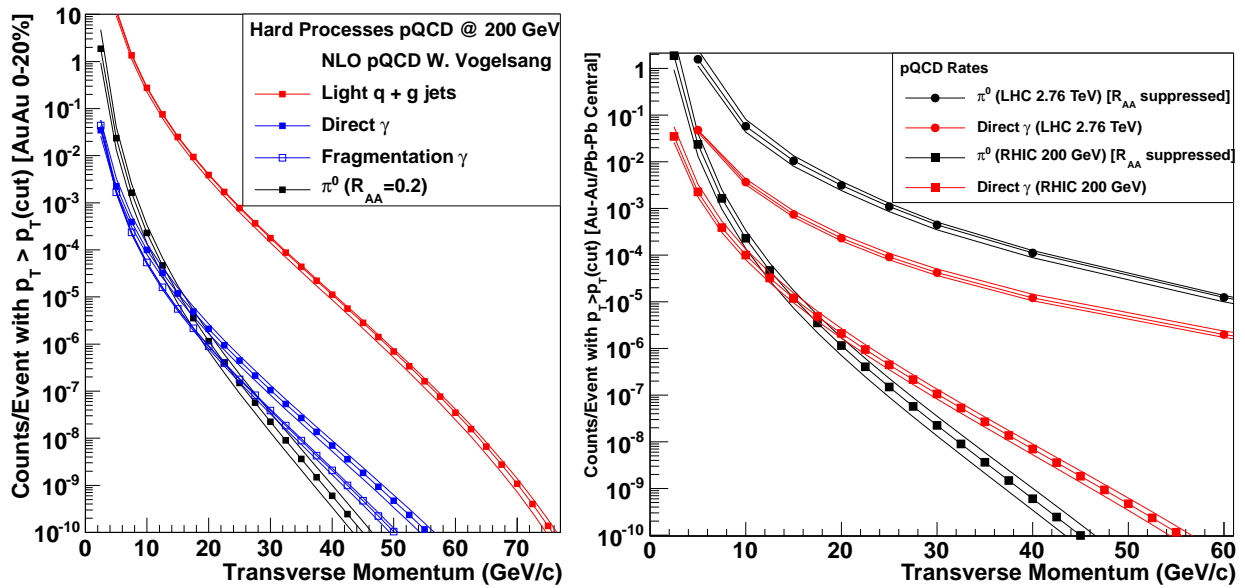
Figure 3.5: (left) Event rates of jet, photon, and π^0 with $|\eta| < 1$ in central (0–20%) Au+Au collisions at 200 GeV. (right) Event rates of direct photon and π^0 with $|\eta| < 1$ in central Au+Au collisions at 200 GeV compared with that of Pb+Pb collisions at the LHC energy.

be placed within the sPHENIX aperture, electron ID of sufficient purity would require both dE/dx and TOF covering the full sPHENIX aperture. Given existing funding and schedule constraint the additional subsystems required to make a sensitive measurement will not be available.

3.7 Commissioning and physics opportunities at 200 GeV

A run plan that includes a short $\sqrt{s} = 200\,\text{GeV}$ $p+p$ and Au+Au run will enable sPHENIX to get an excellent start in the jet physics program envisioned for the 2021–2022 RHIC run. Two of the basic steps one needs to successfully carry out a heavy ion jet physics program are to calibrate the jet energy scale of the detector and understand the heavy ion event that underlies the jet signal. A short two-week 200 GeV Au+Au and 200 GeV $p+p$ run would provide invaluable data early to the jet program. The $p+p$ run is important for enabling the energy calibration of the full sPHENIX detector without the complication of a large underlying event. The jet data recorded in the detector region where the EMCal is instrumented can provide the jet energy scale calibration of the combined HCal and EMCal system.

The key jet measurement components of sPHENIX projected to be available in the 2019 run includes a partial implementation of the EMCal, the full HCal, and the BaBar solenoid. PHENIX plans to commission these available detectors during the BES II running, and at the same time, some commissioning is only possible at the full RHIC collision energy.

The left panel of Figure 3.5 shows the expected event rates of jet, photon, and π^0 in central Au+Au collisions. The full sPHENIX detector can record about 50 billion minimum bias Au+Au events including 10 billion central (0–20%) collisions in a nominal RHIC run of 20 weeks at 200 GeV. This means that it is possible to record 5 billion Minimum Bias (1 billion central) Au+Au events with the partial sPHENIX detector in just two weeks of running. If all of the sPHENIX detectors work well in 2019, such a data set would be invaluable for preparing for future RHIC jet physics runs. The rate of 10^{-9} in the vertical axis of Figure 3.5 corresponds to one jet for two weeks of running. Thus two weeks of running at 200 GeV can provide more than 100K jet samples for $p_T > 30\,\text{GeV}/c$. This large sample of jets will be very useful for the detector calibration. It can also provide possibility of the first jet measurement using hadronic calorimeter at RHIC energy. Since the EMCal is only partially instrumented, the jet energy resolution of the partial sPHENIX is degraded from that of the full sPHENIX. However, it should be sufficient for the first trial of the jet measurement.

In the limited solid angle where EMCal is instrumented, the partial sPHENIX should have the same detector performance as the full sPHENIX. The event rates of the jets whose jet cone ($R \approx 0.2$) is fully contained in the EMCal instrumented region will be less than 10% of that shown in Figure 3.5. However, the event rate in 10% of full sPHENIX acceptance for 2 weeks is 100 million central collisions, which is quite substantial for single jet measurement.

The right panel of Figure 3.5 shows expected events rate of direct photons and π^0 in central Au+Au collisions at 200 GeV. Measurements of direct photons and π^0 requires the EMCal. Thus the event rate in the 2019 run is significantly lower than that in the Figure. Still, with 25% of EMCal instrumented, the number of direct photons in EMCal is approximately 500 for $p_T > 20\,\text{GeV}/c$ in two weeks.

The data set obtained during the full energy run, in particular the data in the fully instrumented region serve for developing data analysis techniques of jet measurements and direct photon measurement with full sPHENIX detector. This would significantly advance the readiness of physics analysis of full sPHENIX detector in the 2021 run.

Chapter 4

Run Plan

In the previous Chapters, we described the physics potential and the detector configurations needed to make the measurements. In this Chapter, we present a strawman for running in the second year of the BES II (2019). The guidance in the Charge for this document was to assume 22-cryo weeks in 2019.

The observables discussed in this document have been chosen because of their potential sensitivity to the onset of deconfinement and the QCD critical end point. Theoretical guidance gives hints that the critical point should be seen within a region spanning $\mu_B = 50$ MeV [33] around the critical value, so energy steps equivalent to this gap in μ_B are necessary. Thus far, PHENIX has taken a low statistics data set at 7.7 GeV, and higher statistics data sets at 19.6 GeV, 39 GeV, and 62.4 GeV. For technical reasons due to limitations of the RHIC collider during Run-10, RHIC was unable to deliver collisions at $\sqrt{s_{NN}} = 11.5$ GeV at both PHENIX and STAR. Clearly publication of all BES I results and initial BES II results from the STAR experiment in 2018 (while PHENIX is still in the decommissioning and installation process) will be extremely informative in optimizing the 2019 run plan.

We propose to cover a number of energies in the BES II range, as well as a short pilot run for $p+p$ and $Au+Au$ at $\sqrt{s_{NN}} = 200$ GeV for the sPHENIX commissioning.

4.1   Collision Energies and Integrated Luminosities

Table 3.1 lists the estimated minimum number of events necessary to make a statistically significant measurement at $\sqrt{s_{NN}} = 19$ GeV for a variety of physics topics relevant to the BES II program. In order to translate these estimates into running time, we have used the luminosity projections shown in Figure 1.1 and tabulated in Table 4.1. Experience from BES I shows that both the recorded event rate and the good event rate drops rapidly as $\sqrt{s_{NN}}$ is decreased below 27 GeV. For BES I the good event rate refers to the rate of

events that can be included in an analysis, factoring in the PHENIX duty factor, cuts on the number of hits in the Beam-Beam Counter, and a cut on the z-vertex requiring events to lie within 30 cm of the nominal collision vertex. Assuming that the sPHENIX trigger detector configuration for BES II is similar to the current configuration, it is the good event rate that represents how much running time is necessary to collect the number of events needed for a given physics analysis. Below a collision energy of 27 GeV, the PHENIX good event rate is observed to drop exponentially with $\sqrt{s_{NN}}$. An exponential fit to the three data sets at which PHENIX has run at these energies (27 GeV, 19.6 GeV, and 7.7 GeV) is used to interpolate the good event rates to the other collision energies. Table 4.1 summarizes the projected PHENIX event rates at a variety of collision energies.

Table 4.1: A summary of the projected RHIC luminosity and the projected PHENIX event rate for BES II. The PHENIX event rate is quoted as millions of events per day for good events that can be used for analysis within $|z_{vertex}| < 30$ cm and includes the PHENIX and RHIC duty factor. The PHENIX event rates for collision energies not covered in Run-10 are obtained from an exponential fit to the rates from the Run-10 data sets.

	Run-10		Run-19 projection		
$\sqrt{s_{NN}}$	rate	$\langle \mathcal{L} \rangle$	rate	$\langle \mathcal{L} \rangle$	gain
GeV	Mevt/day	cm^{-2}s^{-1}	Mevt/day	cm^{-2}s^{-1}	factor
19.6	0.95	4.0×10^{25}	24	1.0×10^{27}	25
15.0	0.35		3.8	2.6×10^{26}	11
13.0	0.26		2.2	1.7×10^{26}	8
11.5	0.17	1.6×10^{25}	1.0	9.1×10^{25}	6
9.0	0.10		0.4	1.2×10^{25}	4
7.7	0.041	1.3×10^{24}	0.13	4.0×10^{24}	3
5.0	0.023		0.05	4.3×10^{23}	2

sPHENIX will participate in at most the 2019 year of the BES II run. Participation in the 2018 run is not possible under the boundary conditions described in this document. Table 4.2 lays out a proposed BES II program request for sPHENIX. The request is possible in a RHIC running period of 22 cryo-weeks including cool down and ramp-up, leaving 19 weeks of physics running. The table lists data sets in order of priority. Higher priority

goes to collision energies at which PHENIX has not yet taken data with a special interest in the region near 11.5 GeV. The request takes care to minimize gaps in μ_B between energies. A short run at 19.6 GeV would be helpful to compare measurements from the baseline sPHENIX detector to measurements from the current PHENIX detector. The request includes four weeks of full energy running split into two weeks of Au+Au and two weeks of $p+p$ running. Running at 5 GeV is given a very low priority since a useful data set would require an impractically long running time. It would take 218 days of running time to record only 10 million events. Therefore, running at 5 GeV is not included in Table 4.2.

As detailed in Section 3.7, we request a short, of order two weeks, of running for $p+p$ and Au+Au at $\sqrt{s_{NN}} = 200$ GeV. This critical pilot data taking would come at a small cost in running time and help ensure a fully successful program for the full sPHENIX starting in 2021.

Table 4.2: An outline of the PHENIX run request for the BES II program. The running time is integrated to cover a single year of RHIC running that spans 22 cryo-weeks, or 19 weeks of physics running depending on ramp-up and switching times. Higher priority is given to the data sets listed first. The number of events refers to good events within the baseline sPHENIX configuration requiring $|z_{vertex}| < 10$ cm including the PHENIX and RHIC duty factor. Also included are event estimates with a wider $|z_{vertex}| < 30$ cm and $|z_{vertex}| < 1$ m cut that could be applied if a TPC is installed.

Species	$\sqrt{s_{NN}}$ (GeV)	μ_B (MeV)	Run Time (Days)	Events(M) $|z_{vtx}| < 10$cm	Events(M) $|z_{vtx}| < 30$cm	Events(M) $|z_{vtx}| < 1$ m
	11.5	315	45	15	45	112.5
	13.0	281	23	17	50	125
Au+Au	9.0	376	41	6	17	42.5
	19.6	205	4	33	100	2500
	200	20	10	1200	3600	9000
p+p	200		10	1.2 pb^{-1}	3.6 pb^{-1}	9 pb^{-1}

Chapter 5

Schedule

Plans are being developed to decommission and remove major elements of the PHENIX detector and to begin the process of sPHENIX detector installation during the 2016–2018 RHIC shutdown period. Given the scale of PHENIX and of sPHENIX, these plans require careful coordination. This Chapter provides a high-level view of the choreography necessary to prepare the detector for BES II in 2019 and the for full sPHENIX running in 2021. More details are also provided in Appendix B. We see the development of a realistic schedule for decommissioning PHENIX and starting the installation of sPHENIX as a key element of our planning for BES II.

Over the next few years, we envision three parallel efforts which will ultimately result in sPHENIX commissioning and data-taking with a partially completed sPHENIX detector during the 2019 RHIC run. The first effort is a continuation of the PHENIX operations and physics activities that have been on-going since the initial RHIC run in 2000. It encompasses data-taking with the current PHENIX experiment during RHIC runs in 2014–2016, normal maintenance and operations activities that support those physics runs and modest upgrades to the PHENIX detector during this period, especially the completion and operation of the MPC-EX subsystem. The work will be carried out by the same team that has been operating PHENIX since 2000, though some group members will be redirected into the other two efforts. This work will be completed at the end of the 2016 run.

The second large project is the planning and carrying-out of the decommissioning of the PHENIX detector. The planning for the decommissioning was begun at the start of 2014 by the PHENIX group and will continue until the end of the 2016 RHIC run as a combined effort of the PHENIX group and the C-AD ES&F group. Major activities associated with PHENIX decommissioning will start at the end of the 2016 run and will continue for approximately one year. Most of the decommissioning work will be carried out by C-AD personnel and outside contractors. Details on this activity can be seen in Appendix B.

The third project is the design, development, construction and installation of sPHENIX itself. The R&D and design work has already begun on this project and is being carried

out by members of the PHENIX collaboration. The project plan anticipates DOE approval of a construction start in FY16.

The tentative funding profile for the sPHENIX MIE is shown in Table 5.1. At the start of the RHIC BES II in 2018 only approximately 40% of the total budget will be available for sPHENIX construction. By the beginning of the 2019 run slightly over 70% of the total sPHENIX budget will have been made available. Under the budget scenario one anticipates being able to build and install by the start of the 2019 run the superconducting magnet infrastructure, the HCal plus a small fraction of the EMCal. We note that RIKEN has agreed to cover the modest cost (< 1 $M) associated with the reconfiguration of the VTX.

Table 5.1: Proposed budget

Budget Year	FY2016	FY2017	FY2018	FY2019	FY2020	Total
Funds in AYM$	4.0	8.0	8.0	6.5	1.4	27.9

The costs associated with the additional detector options are not yet at a stage for inclusion in this document.

Appendix A

BES II Charge

The following pages show the BES II charge to the PHENIX Collaboration from BNL ALD Berndt Mueller.

Charge to PHENIX Collaboration: Update on Plan for Beam Energy Scan II

The current RHIC run plan anticipates the commissioning of bunched beam electron cooling for low energy RHIC beams in FY2017, which will increase the achievable luminosity at low collision energies by up to one order of magnitude (see Figure). After the completion of this upgrade, the present plan envisions carrying out a high statistics beam energy scan (BES-II) with long Au+Au runs at several energies in FY2018 and FY2019 utilizing this new capability.
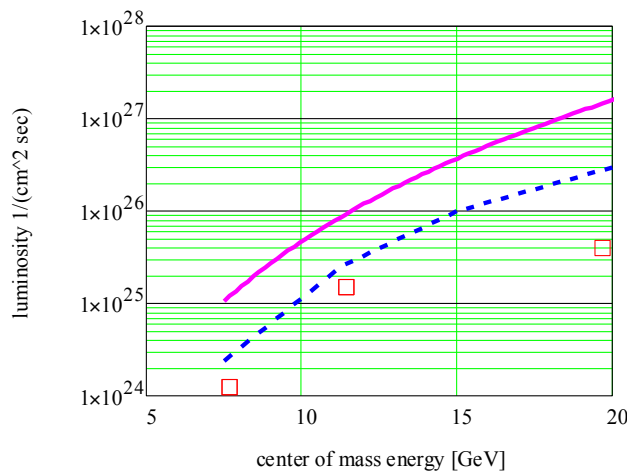

Figure: Projection of average store luminosity within ±1m vertex for 111 bunches of Au ions in RHIC with electron cooling. Red squares: measured average store luminosity in BES-I. Blue dash line: minimum projection of improvement with cooling. Magenta solid line: maximum projection of luminosity improvement with cooling.

Although the 2013 NSAC Future Facilities Report has reaffirmed the central importance of RHIC and its physics program, including the BES-II, I anticipate the need to provide a much more detailed justification of the need for a high statistics beam energy scan in the context of the upcoming Long Range Plan process. It would be good to get ahead of the process and develop an updated plan and justification for the BES-II, which takes into account all that has been learned from the data analysis of BES-I, as well as progress in theory, e.g. lattice simulations at nonzero chemical potential.

I ask you to prepare a White Paper that describes:

- The scientific motivation for the BES-II based on our current knowledge;
- The compelling physics observables and their expected physics reach;
- The desired collision energies and integrated luminosities for each energy;
- The possible need for collision systems other than Au+Au (e.g. p+p);
- The detector requirements for a successful BES-II.

For specificity, you should assume RHIC runs of 22 weeks in each of the years 2018 and 2019. In order make somewhat conservative projections, you should assume a luminosity in the middle between the pessimistic and optimistic projections shown in the Figure.

I would also be interested in an assessment of the detector capabilities to perform meaningful measurements of low-mass dilepton spectra at collision energies where the chiral symmetry breaking transition may be probed.

In order to be most useful as a basis for the discussions in the context of the Long Range Plan process, I request that you submit a BES-II White Paper describing the plans of the PHENIX Collaboration no later than March 1, 2014.

Berndt Mueller

ALD for Nuclear and Particle Physics

October 8, 2013

Appendix B

Decommissioning and Installation Plan

Once the 2016 run is completed the PHENIX group will remove all detector elements in the 1008 Interaction Region (IR) including the East and West Carriages, central spectrometer magnet, Muon Magnet South and Muon Magnet North with their associated detector instrumentation. The equipment remaining in the 1008 IR area at the end of the time will be the MuID steel, MuID detectors captured inside the steel, the steel carriage tracks and the electrical power, water, gas and safety system infrastructure. The decommissioning operation will remove and preserve the beam pipe, racks, and phototubes for future use. Preservation of other PHENIX components such as the EMCal sectors will be considered and if appropriate added to the decommissioning plan as it develops.

The time between the completion of the RHIC 2016 run in late June 2016 and the start of the BES-II run in January 2018 is approximately 80 weeks. The initial decommissioning plan envisions the removal of the existing PHENIX detector and magnets in a seven stage process that takes 50 weeks. The decommissioning stages following the end of the 2016 run are:

1. Area preparation and beam pipe disassembly, removal, and storage

2. East Carriage removal and disposition

3. Muon magnet south removal and disposition

4. Central magnet removal and disposition, VTX/FVTX removal and storage

5. West carriage removal and disposition

6. Muon magnet North Removal and disposition

7. Removal of all remaining extraneous infrastructure including obsolete piping, wiring, fibers and removal of MuID detectors not captured by the MuID steel.

Parallel decommissioning work will be taking place during these 50 weeks in the 1008 Rack Room, Gas Mixing Hut and Gas Pad. The final 30 weeks of the 2016–2017 shut-down will be used to prepare the 1008 IR for sPHENIX and begin installation of specific sPHENIX components. sPHENIX work to be performed during this time include installation of superconducting magnet services particularly the cryo plant, modified and new IR infrastructure (stairways, rails, power supplies, general gas and water plumbing), SC magnet basic support structure and integral sPHENIX detector subassemblies. A detailed decommissioning plan for PHENIX will be developed during 2014 and will include a budget, schedule and list of required resources. It is anticipated that the decommissioning will be carried out by a combination of the PHENIX technical support group, C-AD Experimental Support and Facilities personnel, BNL trades and outside contractors specializing in rigging and salvage.

Disassembly and disposition plans will be developed for each subsystem and carriage. It will contain a list of necessary tools, fixtures, scaffolding, special equipment and personnel. The method of disposition for all parts will be identified. Tasks requiring outside contractors such as specialized rigging will be determined. Areas for transient storage of parts waiting for disposal or transfer off-site will be identified. Areas for long term storage of components that will be reused in sPHENIX or potentially a future eRHIC detector will also be identified. PHENIX components such as the Be beam pipe, silicon vertex detector, electronics racks, phototubes and possibly the Pb Glass calorimeter will need a temporary home for two to four years.

There are a number of constraints and issues that the PHENIX decommissioning plan must address. The PHENIX deconstruction should not require the disassembly of the permanent radiation shield wall in 1008. This implies that all racks on the Central Magnet bridge must be removed prior to the movement of the CM out of the IR. The carriage tracks should remain in their current position since they will be integral to sPHENIX installation. Items such as the Be beam pipe, subsystem PMTs, silicon vertex detector, and electronics racks must be removed and safely stored. Objects such as the central magnet will need to be disassembled in the PHENIX Assembly Hall prior to removal and final disposition but large components of it weight much more that the building crane capacity. A practical rigging solution will need to be identified. The Muon Magnet North is mounted to the floor in the PHENIX hall and has many components weighing over the capacity of the crane in the PHENIX IR. A solution for its removal possibly involving cutting up the MMN in situ will need to be identified. The location of the MuID steel absorber plates is not conflict with either sPHENIX or a potential future ePHENIX detector, and will not be removed during PHENIX decommissioning. However the first layer of MuID North and South is accessible and will be removed. 1008 facility infrastructure such as electrical, water, cooling and safety system services will be preserved as much as practical so that they are available for re-use by sPHENIX without requiring a major rebuild.

Tables B.1 and B.2 detail the current concept of decommissioning activities of PHENIX in 2016 and 2017. Table B.3 lists the activities associated with sPHENIX installation in 2017 and 2018 in preparation for the second year of the BES-II in 2019.

Table B.1: PHENIX Decommissioning tasks and schedule 2016

Tasks	Dates	Details
Preparation	6/27-7/8	Purge flammable gas. Disconnect all gas lines, MuID collars, move MMS, disconnect and move east carriage
Beampipe	7/11-7/22	Beampipe disconnect and move MMS to AH, disassemble beam pipe and move to safe storage
East Carr	7/24/-9/16	Remove, strip and salvage racks and, remove east DC, PC1, PC3, Rich, EM Cal, PbSc & PbGl, TOF and TEC; Salvage PMT's, disassemble EC carriage, dispose/recycle materials
Muon Magnet S	9/19-11/11	Move MMS to AH, remove, strip and salvage racks and, remove south platforms, MPC-Ex, MPC, MuTr Sta. 1, lampshades, MuTr stations 2 and 3,disassemble MMS, dispose/recycle materials
Central Magnet	11/14-1/6	Remove, strip and salvage racks and, remove bridge platforms, RPC1 North and South, BBC North and South, RPC1 Stainless shields, disassemble CM, dispose/recycle materials

Table B.2: PHENIX Decommissioning tasks and schedule 2017

Tasks	Dates	Details
West Carr	1/9-3/3	Move WC to AH, remove, strip and salvage racks, remove west DC, PC1, PC2, PC3, RICH, EM Cal, PbSc, TOF and Aerogel; Salvage PMT's, disassemble WC carriage, dispose/recycle materials
Muon Magnet N	3/6-4/28	Remove, strip and salvage racks and, remove north platforms, MPC-Ex, MPC, MuTr Sta. 1, lampshades, MuTr stations 2 and 3,disassemble MMN, dispose/recycle materials
Other IR Tasks	5/1-5/26	Remove all unneeded Remove all MuID detectors not entrapped in MuID steel and dispose, remove and dispose all obsolete piping, wiring and fibers from IR and AH
Other 1008 Tasks	Jul 2016-Dec 2017	Rack Room, GMH and Gas Pad decommissioning

Table B.3: sPHENIX Installation Tasks and Schedule 2017–2018

Dates	Details
5/29/2017–12/29/2017	Install new and modified IR infrastructure, SC Magnet base and magnet, cryo services. Initial sPHENIX SC Magnet tests and sPHENIX detector subsystem assembly and test take place at BNL location not away from 1008
1/2/2018–12/30/2018	Transport completed HCal, EMCal and VTX to 1008, install sPHENIX modules in and around magnet, install any additional detector systems for BES-II, test all services and components

B.1   Support Infrastructure

The 1008 facility has been operating in the support of the PHENIX Experiment since 2000. The existing complex has infrastructure that supplies approximately 1.2 MW of power to the PHENIX magnets, electronics and building operations. It has large cooling towers for the supply of chilled water, a 6000 gallon N2 dewar, a gas facility that can supply large quantities of argon, CO_2, and a variety of flammable gases, and a gas mixing and control building for the supply of high purity specialty gases. The PHENIX IR and Assembly Hall (AH) have respectively a 10 ton and 40 ton crane. The experimental area is equipped with safety systems that detect fire, smoke, flammable gas, ODH and water leaks which are integrated into an alarm and interlock protection system. The complex also contains a large data acquisition, control and computing complex, high bandwidth connectivity to the RHIC Computing Facility and a Control Room that enables 20–25 scientists and engineers to simultaneously monitor and control the PHENIX experiment. The capabilities of the 1008 complex will remain in place with appropriate improvements during this period.

An important addition to the 1008 area that will be necessary for sPHENIX is cryogenic supply and control for the BaBar magnet. The superconducting solenoid is a 1.5 Tesla magnet with a 1400mm inner cryostat radius, 1730mm outer cryostat radius and 3850mm cryostat length. The existing cryostat incorporates support mounts that will be adapted to the sPHENIX hadronic calorimeter to serve as the flux return. The existing services and vent stack may be modified to exit at an angle outside the acceptance beyond the south end of the HCal detector to cryogenic supply lines, power supplies and monitoring equipment. The existing rigging fixtures from SLAC will be adapted for transport, lifting

and installation. Personnel from the BNL Magnet Division and C-AD will be responsible for integrating the solenoid into the RHIC cryogenic infrastructure.

Major components of sPHENIX will be built at an assembly facility on BNL site and brought to the 1008 Hall for final assembly into sPHENIX. The detector will be positioned on a movable custom carriage mounted to the existing PHENIX rail system or a modification version of the rails. The rail system will be used to move sPHENIX from the assembly hall to the interaction region. Detector assembly, or disassembly as needed during maintenance periods, will be done using the existing cranes.

Appendix C

Developing Technology Considerations

There are a number of detector technologies that are being investigated with active R&D programs by PHENIX collaborators as well as others around the world. Though the technologies described need further development and proof-of-performance on the prototype level before being seriously considered, they each offer potentially interesting capabilities to the sPHENIX detector. With a proof-of-performance and a path for funding yet to be established, it is too early to consider these viable subsystem options. However, the two enhancement options (Fast Time-of-Flight and Compact Cherenkov) described below is considered to have sufficient potential to warrant future consideration if R&D proves them to be practical.

Fast Time-of-Flight

Generally detector R&D in particle and nuclear physics is targeted at a particular application or specific experiment/facility with little work done on purely generic detector R&D. An exception to this rule is the highly-touted LAPPD (Large Area Picosecond Photon Detection) work that is currently proceeding under the leadership of University of Chicago and Argonne National Laboratory. The essential principle of the LAPPD is to avalanche photon-electrons originating from Cherenkov light with a narrow transit time spread. The latter is achieved by minimizing the size of the avalanche structure. Recent advances in the production of micro-channel plates based upon "fused fibers" along with new ALD (Atomic Layer Deposition) coating techniques have demonstrated laboratory performance at or below $\sigma \sim 10 \ psec$.

The LAPPD project is attempting to enter Phase-II via an SBIR with the Incom company to bring production of these units into the commercial sector. Although the commercial venture will target low cost devices, it is difficult to speculate on the final cost per m^2 of this technology. Additionally, the high resolution timing can only be exploited by electronics of sufficient precision.

In addition to the central LAPPD effort, a funded project under the banner of EIC R&D has just been initiated. In addition to direct time-of-flight measurements, this detector technology may be ideal for readout of aerogel detectors, which are part of many Electron Ion Collider (EIC) detector designs, including the ePHENIX design in the hadron-going direction.

The potential resolution of these devices should be more than sufficient to provide effective electron identification capabilities when combined with dE/dx information from a TPC. However, an application relevant to the BES II running period could be time-of-flight in the forward direction if a suitable tracking solution were to emerge. Figure C.1 shows the performance of a 10 psec TOF wall located 1 meter or 4 meters from the collision point.
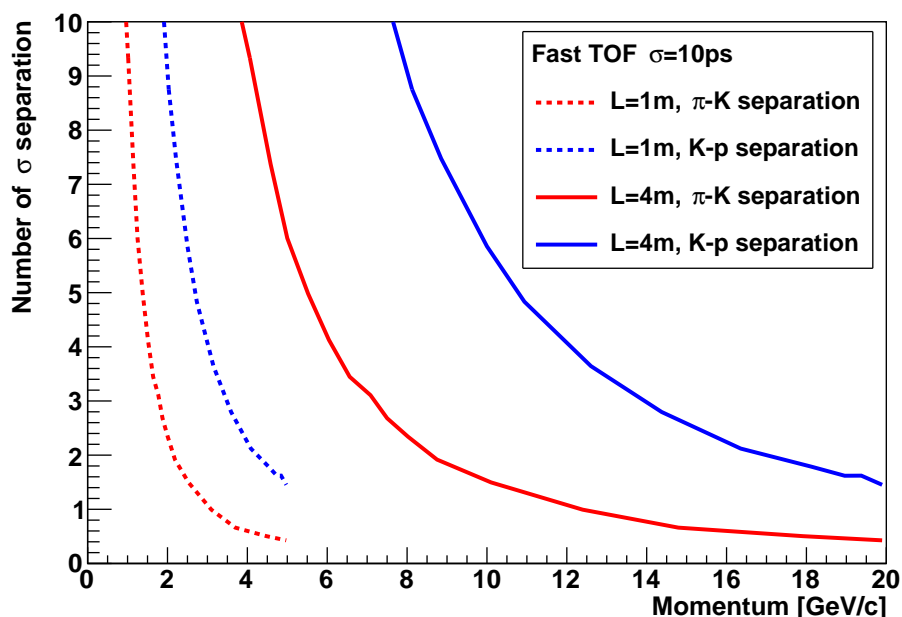

Figure C.1: Hadron identification performance of a forward time-of-flight wall with 10 picosecond resolution located 1 meter (or 4 meters) from the collision point.

Compact Cherenkov Detector

A time projection chamber (TPC) provides good particle identification at low momentum by measuring ionization (dE/dx) left by charge particles in the TPC gas volume. The physics program of sPHENIX/ePHENIX experiments can significantly benefit from the particle identification enhancement to higher p in the rapidity coverage of the TPC.

Identifying particles at higher momentum can be done with Cherenkov detectors using solid state radiators. LiF and MgF_2 materials are transparent down to the wavelengths

of 105-115 nm, where CsI photocathode reaches $> 80\%$ quantum efficiency. Using CsI evaporated on the top of the GEM surface [34] allow to obtain hundreds of photoelectrons from 1 cm of radiator length. Such approach may allow building compact Cherenkov detector which can be placed just after the TPC. Again R&D in this direction is currently ongoing.

Bibliography

[1] C. Aidala, N.N. Ajitanand, Y. Akiba, Y. Akiba, R. Akimoto, et al. sPHENIX: An Upgrade Concept from the PHENIX Collaboration. 2012. `arXiv:1207.6378`. (document), 2, 2.1

[2] E. O'Brien. Recent PHENIX results from the RHIC energy scan. *Nucl. Phys.*, A904-905:264c–269c, 2013. `doi:10.1016/j.nuclphysa.2013.01.071`. (document)

[3] A. Adare et al. Concept for an Electron Ion Collider (EIC) detector built around the BaBar solenoid. 2014. `arXiv:1402.1209`. (document)

[4] R.A. Bell et al. The BaBar superconducting coil: Design, construction and test. *Nucl. Phys. Proc. Suppl.*, 78:559–564, 1999. `doi:10.1016/S0920-5632(99)00603-9`. 2.1

[5] M. Shao, O. Barannikova, X. Dong, Y. Fisyak, L. Ruan, et al. Extensive particle identification with TPC and TOF at the STAR experiment. *Nucl. Instrum. Meth.*, A558:419–429, 2006. `arXiv:nucl-ex/0505026, doi:10.1016/j.nima.2005.11.251`. 2.4

[6] L Musa and K Safarik. Letter of Intent for the Upgrade of the ALICE Experiment. Technical Report CERN-LHCC-2012-012. LHCC-I-022, CERN, Geneva, Aug 2012. 2.4

[7] M. Asakawa and K. Yazaki. Chiral Restoration at Finite Density and Temperature. *Nucl. Phys.*, A504:668–684, 1989. `doi:10.1016/0375-9474(89)90002-X`. 3

[8] Y. Aoki, G. Endrodi, Z. Fodor, S.D. Katz, and K.K. Szabo. The Order of the quantum chromodynamics transition predicted by the standard model of particle physics. *Nature*, 443:675–678, 2006. `arXiv:hep-lat/0611014, doi:10.1038/nature05120`. 3

[9] S. Ejiri. Canonical partition function and finite density phase transition in lattice QCD. *Phys.Rev.*, D78:074507, 2008. `arXiv:0804.3227, doi:10.1103/PhysRevD.78.074507`. 3

[10] M. A. Stephanov. QCD phase diagram and the critical point. *Prog.Theor.Phys.Suppl.*, 153:139–156, 2004. `arXiv:hep-ph/0402115, doi:10.1142/S0217751X05027965`. 3

[11] J.D. Bjorken. Highly Relativistic Nucleus-Nucleus Collisions: The Central Rapidity Region. *Phys. Rev.*, D27:140–151, 1983. `doi:10.1103/PhysRevD.27.140`. 3.1

[12] J.T. Mitchell. PHENIX Experiment Results from the RHIC Beam Energy Scan Program. 2013. `arXiv:1308.2185`. 3.1

[13] J.T. Mitchell. The RHIC Beam Energy Scan Program: Results from the PHENIX Experiment. *Nucl. Phys.*, A904-905:903c–906c, 2013. `arXiv:1211.6139,doi:10.1016/j.nuclphysa.2013.02.161`. 3.1

[14] E. Schnedermann, J. Sollfrank, and U. W. Heinz. Thermal phenomenology of hadrons from 200-A/GeV S+S collisions. *Phys.Rev.*, C48:2462–2475, 1993. `arXiv:nucl-th/9307020,doi:10.1103/PhysRevC.48.2462`. 3.2

[15] M. Gazdzicki and M. I. Gorenstein. On the early stage of nucleus-nucleus collisions. *Acta Phys.Polon.*, B30:2705, 1999. `arXiv:hep-ph/9803462`. 3.2

[16] S. Wheaton and J. Cleymans. THERMUS: A Thermal model package for ROOT. *Comput.Phys.Commun.*, 180:84–106, 2009. `arXiv:hep-ph/0407174,doi:10.1016/j.cpc.2008.08.001`. 3.2

[17] A. Adare et al. Evolution of π^0 suppression in Au+Au collisions from $\sqrt{s_{NN}} =$ 39 to 200 GeV. *Phys.Rev.Lett.*, 109:152301, 2012. `arXiv:1204.1526,doi:10.1103/PhysRevLett.109.152301`. 3.2

[18] A. Adare et al. J/ψ suppression at forward rapidity in Au+Au collisions at $\sqrt{s_{NN}} = 39$ and 62.4 GeV. *Phys.Rev.*, C86:064901, 2012. `arXiv:1208.2251,doi:10.1103/PhysRevC.86.064901`. 3.2

[19] S. Horvat. Charged Hadron Nuclear Modication Factors in the Beam Energy Scan from STAR. *PoS*, CPOD2013:002, 2013. 3.2, 3.2

[20] R. A. Lacey, R. Wei, N.N. Ajitanand, and A. Taranenko. Initial eccentricity fluctuations and their relation to higher-order flow harmonics. *Phys.Rev.*, C83:044902, 2011. `arXiv:1009.5230,doi:10.1103/PhysRevC.83.044902`. 3.3

[21] R. A. Lacey, N.N. Ajitanand, J.M. Alexander, P. Chung, J. Jia, et al. An Estimate for the location of QCD critical end point. 2007. `arXiv:0708.3512`. 3.3

[22] R. A. Lacey, A. Taranenko, J. Jia, D. Reynolds, N.N. Ajitanand, et al. Beam energy dependence of the viscous damping of anisotropic flow. 2013. `arXiv:1305.3341`. 3.3

[23] D. T. Son and A. O. Starinets. Minkowski space correlators in AdS / CFT correspondence: Recipe and applications. *JHEP*, 0209:042, 2002. `arXiv:hep-th/0205051,doi:10.1088/1126-6708/2002/09/042`. 3.4

[24] D. Kharzeev, A. Krasnitz, and R. Venugopalan. Anomalous chirality fluctuations in the initial stage of heavy ion collisions and parity odd bubbles. *Phys.Lett.*, B545:298–306, 2002. `arXiv:hep-ph/0109253,doi:10.1016/S0370-2693(02)02630-8`. 3.4

[25] P. B. Arnold and G. D. Moore. QCD plasma instabilities: The NonAbelian cascade. *Phys.Rev.*, D73:025006, 2006. `arXiv:hep-ph/0509206, doi:10.1103/PhysRevD.73.025006`. 3.4

[26] Misha A. Stephanov, K. Rajagopal, and Edward V. Shuryak. Event-by-event fluctuations in heavy ion collisions and the QCD critical point. *Phys. Rev.*, D60:114028, 1999. `arXiv:hep-ph/9903292, doi:10.1103/PhysRevD.60.114028`. 3.5, 3.5.2

[27] F. Karsch and K. Redlich. Probing freeze-out conditions in heavy ion collisions with moments of charge fluctuations. *Phys.Lett.*, B695:136–142, 2011. `arXiv:1007.2581, doi:10.1016/j.physletb.2010.10.046`. 3.5

[28] B. Berdnikov and K. Rajagopal. Slowing out-of-equilibrium near the QCD critical point. *Phys.Rev.*, D61:105017, 2000. `arXiv:hep-ph/9912274, doi:10.1103/PhysRevD.61.105017`. 3.5

[29] M.A. Stephanov. Non-Gaussian fluctuations near the QCD critical point. *Phys.Rev.Lett.*, 102:032301, 2009. `arXiv:0809.3450, doi:10.1103/PhysRevLett.102.032301`. 3.5

[30] M.A. Stephanov. Evolution of fluctuations near QCD critical point. *Phys.Rev.*, D81:054012, 2010. `arXiv:0911.1772, doi:10.1103/PhysRevD.81.054012`. 3.5

[31] Y. Hatta and M.A. Stephanov. Proton number fluctuation as a signal of the QCD critical endpoint. *Phys.Rev.Lett.*, 91:102003, 2003. `arXiv:hep-ph/0302002, doi:10.1103/PhysRevLett.91.102003`. 3.5

[32] L. Adamczyk et al. Energy Dependence of Moments of Net-proton Multiplicity Distributions at RHIC. *Phys.Rev.Lett.*, 112:032302, 2014. `arXiv:1309.5681, doi:10.1103/PhysRevLett.112.032302`. 3.5.1

[33] Y. Hatta and T. Ikeda. Universality, the QCD critical / tricritical point and the quark number susceptibility. *Phys.Rev.*, D67:014028, 2003. `arXiv:hep-ph/0210284, doi:10.1103/PhysRevD.67.014028`. 4

[34] W. Anderson et al. Design, construction, operation and performance of a Hadron Blind Detector for the PHENIX experiment. *Nucl. Instrum. Meth.*, A646(1):35 – 58, 2011. URL: `http://www.sciencedirect.com/science/article/pii/S0168900211007534, doi:http://dx.doi.org/10.1016/j.nima.2011.04.015`. C